Full Title: Facial shape and allometry quantitative trait locus intervals in the Diversity Outbred mouse are enriched for known skeletal and facial development genes

Short title: The genetics of mouse facial shape variation

Authors

David C. Katz[1*], J. David Aponte[1], Wei Liu[1], Rebecca M. Green[1], Jessica M. Mayeux[2], K. Michael Pollard[2], Daniel C. Pomp[3], Steven C. Munger[4], Steven A. Murray[4], Charles C. Roseman[5], Christopher J. Percival[6], James Cheverud[7], Ralph S. Marcucio[8], Benedikt Hallgrímsson[1*]

Affiliations

[1] Department of Cell Biology & Anatomy, Alberta Children's Hospital Research Institute and McCaig Bone and Joint Institute, Cumming School of Medicine, University of Calgary, AB, Canada

[2] Department of Molecular Medicine, The Scripps Research Institute, La Jolla, CA, USA

[3] Department of Genetics, University of North Carolina Medical School, Chapel Hill, NC, USA

[4] The Jackson Laboratory, Bar Harbor, ME, USA

[5]Department of Animal Biology, University of Illinois Urbana Champaign, Urbana, IL, USA

[6] Department of Anthropology, Stony Brook University, Stony Brook, NY, USA

[7] Department of Biology, Loyola University Chicago, Chicago, IL, USA

[8] Department of Orthopaedic Surgery, School of Medicine, University of California San Francisco, San Francisco, CA, USA

*** Corresponding authors**

bhallgri@ucalgary.ca, david.katz@ucalgary.ca

Author contributions

Conceptualization (Katz, Aponte, Hallgrimsson, Cheverud, Roseman); Data Curation (Pomp, Murray, Pollard, Munger, Mayeux, Liu, Katz); Formal analysis (Katz); Funding acquisition (Hallgrimsson); Investigation (Mayeux, Aponte, Katz, Liu); Methodology (Percival, Aponte, Green, Katz, Cheverud, Roseman, Hallgrimsson); Resources (Murray, Pomp, Pollard, Munger); Supervision (Cheverud, Roseman, Hallgrimsson); Writing—Original Draft: Katz; Writing—Review and Editing: Everyone.

Abstract

The biology of how faces are built and come to differ from one another is complex. Discovering the genes that contribute to differences in facial morphology is one key to untangling this complexity, with important implications for medicine and evolutionary biology. This study maps quantitative trait loci (QTL) for skeletal facial shape using Diversity Outbred (DO) mice. The DO is a randomly outcrossed population with high heterozygosity that captures the allelic diversity of eight inbred mouse lines from three subspecies. The study uses a sample of 1147 DO animals (the largest sample yet employed for a shape QTL study in mouse), each characterized by 22 three-dimensional landmarks, 56,885 autosomal and X-chromosome markers, and sex and age classifiers. We identified 37 facial shape QTL across 20 shape principal components (PCs) using a mixed effects regression that accounts for kinship among observations. The QTL include some previously identified intervals as well as new regions that expand the list of potential targets for future experimental study. Three QTL characterized shape associations with size (allometry). Median support interval size was 3.5 Mb. Narrowing additional analysis to QTL for the five largest magnitude shape PCs, we found significant overrepresentation of genes with known roles in growth, skeletal development, and sensory organ development. For most intervals, one or more of these genes lies within 0.25 Mb of the QTL's peak. QTL effect sizes were small, with none explaining more than 0.5% of facial shape variation. Thus, our results are consistent with a model of facial diversity that is influenced by key genes in skeletal and facial development and, simultaneously, is highly polygenic.

Author Summary

The mammalian face is a complex structure serving many functions. We studied the genetic basis for facial skeletal diversity in a large sample of mice from an experimental population designed for the study of complex traits. We quantified the contribution of genetic variation to variation in three-dimensional facial shape across more than 55,000 genetic markers spread throughout the mouse genome. We found 37 genetic regions which are very likely to contribute to differences in facial shape. We then conducted a more detailed analysis of the genetic regions associated with the most variable aspects of facial shape. For these regions, a disproportionately large number of genes are known to be important to growth and to skeletal and facial development. The magnitude of these genetic contributions to differences in facial shape are consistently small. Our results therefore support the notion that facial skeletal diversity is influenced by many genes of small effect, but that some of these small effects may be related to genes that are fundamental to skeletal and facial development.

Introduction

The facial skeleton is a complex morphology that serves a diverse set of critical roles. It houses and protects the forebrain and most sensory organs and provides essential anatomy for oral communication, feeding, and facial expression. Structured differences (covariance) in facial shape and form depend upon variation in the biological processes that coordinate facial development [1-7]. Understanding how these processes act and combine to build a facial skeleton requires interrogation at multiple levels of the genotype-phenotype (GP) map [8, 9].

Among the most fundamental of these inquiries is the search for genetic variants that contribute to facial variation. These genetic variants are the basic building blocks of diversity

80 and, within species, circumscribe the potential for short-term evolutionary change [10, 11].
81 Over the past decade, dozens of studies in humans, mouse models, and other species have
82 dissected GP associations for the craniofacial complex using moderate-to-high density genetic
83 maps (tens of thousands to millions of markers). The focus is typically on additive effects [12],
84 though some recent work considers interactions among loci [4, 13, 14].
85 In humans, genome-wide association studies (GWAS) targeting variation in soft tissue
86 facial form have been completed for European [15-20], African [21], South American [22], and
87 Asian [23] cohorts. Collectively, the studies report around 50 loci for facial morphology [24].
88 While there is limited overlap in the candidate gene sets among studies [25], and though many
89 of the individual genes have no previously known role in facial development [3], the genes that
90 do replicate across GWAS (*PAX 1*, *PAX3, HOXD* cluster genes, *DCHS2*, *SOX9*) are known to be
91 important to facial and/or skeletal morphogenesis.
92 Compared to human studies, mapping the genetics of facial variation in mice offers
93 several benefits, including greater control over genetic and environmental variation and the
94 ability to record observations, directly or *in silico*, on the skeleton itself [14, 26-31]. In recent
95 years, the focus of mouse skull QTL analyses has expanded to include tests of enrichment for
96 disease phenotypes and roles in skull development, as well as the search for and validation of
97 candidate genes [32-34]. Dozens of QTL have been identified. As with human facial shape
98 GWAS candidates, this is encouraging but also a small beginning—on the order of the total
99 number of loci identified for human height just a decade ago [35]. Quantitative genetics
100 analyses [32, 36, 37] and expression and epigenomic atlases of facial development both
101 strongly point to the potential for hundreds or thousands of genetic loci with as-yet-undetected

102 QTL variance contributions [38-40]. Increased sample sizes, greater mapping resolution, and the
103 development of new experimental lines all have the potential to expand the facial shape QTL
104 library and increase the precision of variant localization [41-43].

105 The present study maps mouse facial shape QTL in what is, to date, the largest sample
106 yet used for this purpose (*n* = 1147). We use Diversity Outbred mice (DO; Jackson Laboratory,
107 Bar Harbor, ME), a random outcross model derived from the Collaborative Cross (CC) founding
108 lines [43-46]. The DO is specifically designed for genetic mapping of complex traits. Each
109 animal's genome is a unique mosaic of the genetic diversity present in the CC founders—more
110 than 45 million segregating SNPs [47]. Random outcrossing (of non-sibs) over many DO
111 generations maintains this diversity and increases recombination frequency, which is critical for
112 reducing confidence intervals of localized QTL [41]. Compared to classic backcross and
113 intercross designs, the combinatorial possibilities for allelic variation within and among DO
114 animals are vast. The genetic diversity in a DO sample may thus mimic diversity in the natural
115 populations that animal models are meant to illuminate.

116 We quantify facial shape with 22 three-dimensional landmarks **(Fig 1)** and estimate its
117 association with founder haplotype variation at 56,885 genetic markers. The dependent
118 observations in the QTL scans are scores on shape PCs. For each PC explaining more than 1% of
119 shape variation, we identify statistically significant marker effects using a mixed effects
120 regression model that simultaneously accounts for kinship among animals [48, 49]. We then
121 undertake a more detailed analysis of QTL intervals for shape PCs 1-5. We estimate founder
122 coefficients, test whether the overall gene set is enriched for biological processes relevant to
123 facial development and perform association mapping to highlight a list of potential causal

genes. In order to visualize and quantify the magnitude of marker effects on multivariate facial shape (as opposed to univariate PC scores), for each QTL peak, we fit an additional mixed model that accommodates high-dimensional dependent observations [50].

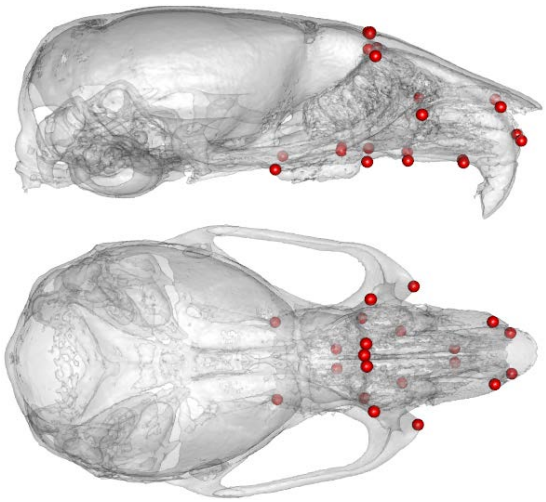

Fig 1. Landmark map.

Results and Discussion

QTL and Shape Variable Heritability

We used a mixed effects regression model to quantify GP associations between 56,885 genetic markers and each of the 20 shape PCs explaining >1% of the symmetric component of facial shape variation **(S1 Fig)**. Evidence for a QTL was evaluated by comparing logs odds (LOD) scores (likelihood ratios comparing the magnitude of marker model residuals to the residuals of a null model that excludes the marker effect) [51] at each marker to a distribution of maximum LOD scores obtained from quantifying marker effects over 1000 random permutations of GP assignments.

While comparisons to prior studies are complicated by design features unique to each, the design employed here appears to have conferred benefits in terms of QTL identification and localization, the primary objectives of QTL analysis [41]. From the 20 genome scans, 37 QTL

surpassed our threshold for statistical significance (95% quantile of the maximum LOD score distribution). Median support interval width was 3.5 Mb (mean 7.1 Mb) using a 1.5 LOD-drop threshold to define support interval boundaries. Comparable prior studies identified 17-30 QTL for the skull, with a lowest median QTL interval of 7.8 Mb (using a less-demanding 1.0 LOD-drop threshold) [32, 33].

Fig 2 plots the support intervals for these QTL (**see also S1 Table**). The QTL span 15 of 19 autosomes as well as the X-chromosome. On chromosomes 7, 14, 15, and 17, QTL from multiple PCs have overlapping associations with the same genomic region.

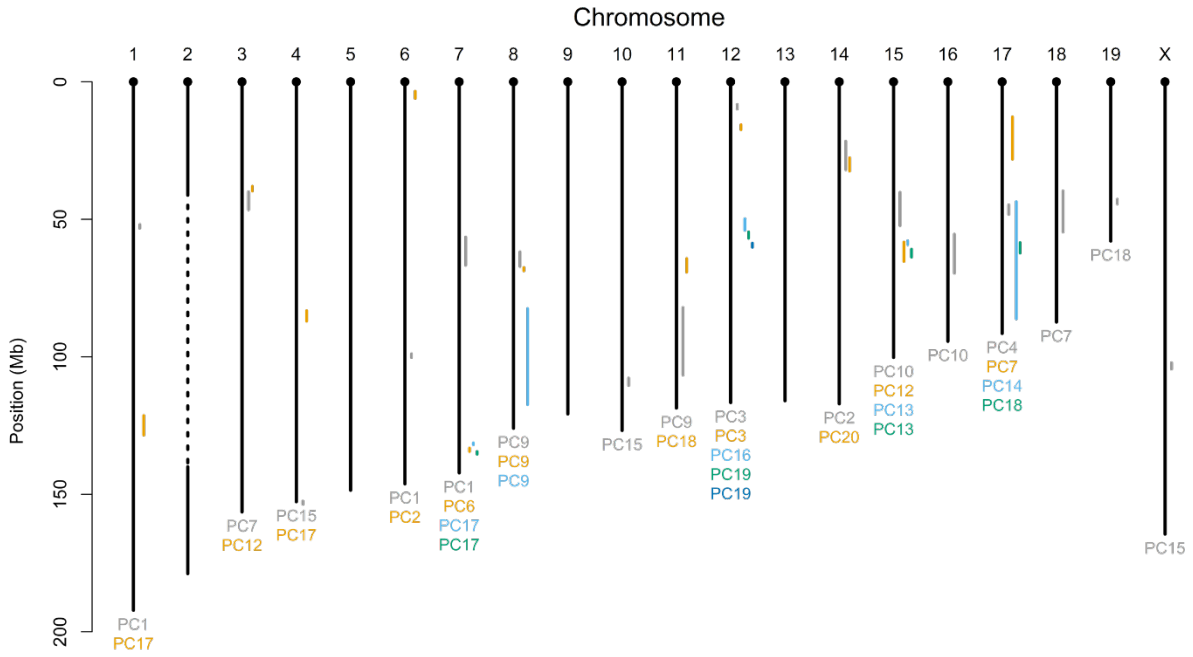

Fig 2. Mouse genome physical map with QTL support intervals. Intervals on the same chromosome are color coded to match the color of the PC for which the QTL was identified (listed below chromosome). The dashed line in the middle of chromosome 2 represents a region for which genetic effects were not evaluated due to the potential effects of transmission distortion on QTL identification (see Materials & Methods for further explanation).

158 For each PC, the random effect heritability estimate quantifies the proportion of
159 phenotypic variance attributable to overall genetic similarity at the founder level [49]. We
160 excluded from the genetic similarity (relatedness) calculation all markers on the same
161 chromosome as the QTL marker of interest. This leave-one-chromosome-out (LOCO) strategy
162 was chosen in order to avoid the loss of power that can arise when relatedness is computed
163 from the full complement of genotyped markers [52-54]. The LOCO approach produces a
164 unique heritability estimate for each chromosome on each PC. **Table 1** reports the mean
165 heritability for each PC, as well as the variance in these heritabilities (averaged over
166 chromosomes). For most PCs, heritability was moderately high (0.42-0.57), with a few low
167 heritability outliers. These values are very similar to those Pallares and colleagues estimated for
168 skull shape PCs in an outbred mouse sample [32], and lie mostly in the middle of the heritability
169 range for human facial shape (~30-70%) [36, 55].
170 **Table 1. Heritabilities by PC.**

	Mean h^2	Variance
PC1	0.5407	0.00012
PC2	0.4389	0.00013
PC3	0.5418	0.00022
PC4	0.3532	0.00022
PC5	0.4627	0.00012
PC6	0.5705	0.00015
PC7	0.4785	0.00014
PC8	0.4604	0.00015
PC9	0.5411	0.00032
PC10	0.5420	0.00017
PC11	0.2439	0.00009
PC12	0.4226	0.00014
PC13	0.5309	0.00013
PC14	0.4364	0.00020
PC15	0.4849	0.00005
PC16	0.4456	0.00010
PC17	0.4658	0.00020
PC18	0.4726	0.00019
PC19	0.4533	0.00006
PC20	0.5040	0.00022

Mean and variance of heritability for PC 1-20 shape traits. The full set of heritability estimates is provided in **S2 Table**.

Based on signal-to-noise evaluation of shape PC eigenvalue decay [56], we limited further analysis to the first five PCs (effectively four PCs, as no marker exceeded the permutation significance threshold for the PC 5 shape axis). Each plot in **Fig 3** depicts the LOD score profile (lower panel) and CC founder haplotype coefficients (upper panel) for a chromosome harboring one or more QTL for a PC 1-4 shape variable. Shaded rectangular regions delimit the 1.5-LOD drop support interval boundaries for the QTL. Founder coefficients were estimated using best linear unbiased predictors [57, 58]. This helps to highlight QTL regions by imposing a degree of shrinkage on the coefficients chromosome-wide [48].

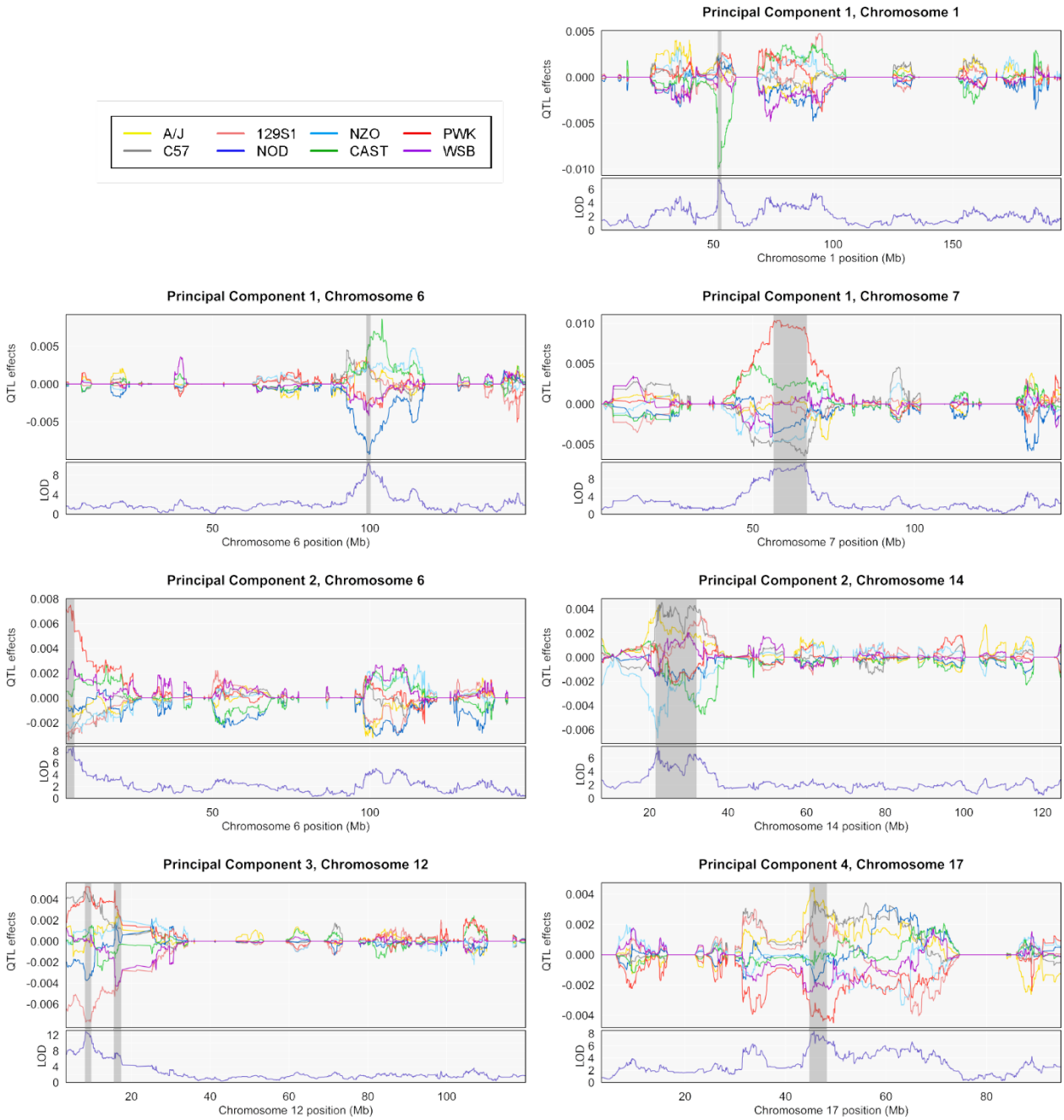

Fig 3. BLUP effects and LOD panels for all QTL, PCs 1-4. QTL effect colors correspond to CC founders.

We also mapped GP associations for vectors capturing covariation between shape and two measures of size: centroid size (CS) and body mass. Shape change associated CS and body mass variation were closely correlated with the primary axis of shape variation in our sample

190 ($r_{PC1\text{-}CS}$: 0.985, $r_{PC1\text{-}Mass}$: 0.875, $r_{CS\text{-}Mass}$: 0.927). These correlations carry forward to the QTL

191 profiles, as well. We identify two QTL each for CS and body mass allometry, one of which, on

192 chromosome 6, is common to the two allometry vectors. Together, the three QTL—on

193 chromosomes 1, 6, and 7—completely overlap with the PC 1 shape QTL (**Fig 4**).

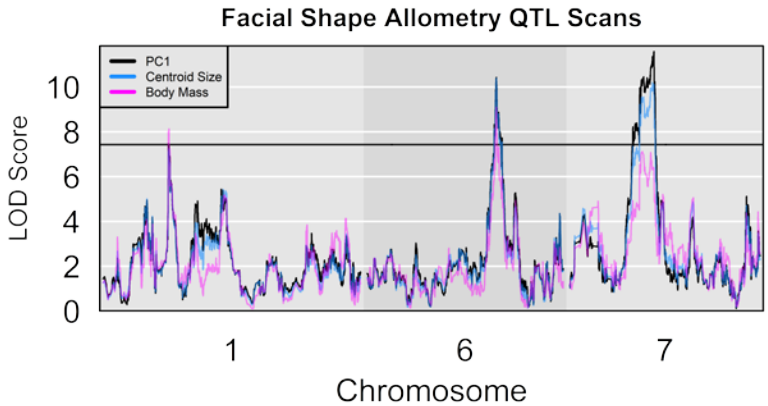

194
195 **Fig 4.** LOD plots for chromosomes containing allometry (CS and body mass) and PC 1
196 QTL. The permutation significance thresholds for all three phenotypic variables are
197 extremely similar. Only one is plotted.
198
199 The allometry results suggest a developmental model in which the determinants of

200 different size measures have partially correlated effects on cranial shape [59]. The near

201 coincidence of shape PC 1 with our explicitly allometric variables has been observed in many

202 geometric and classical morphometric investigations, and there is a long history of treating PC 1

203 as an allometry variable in morphometric analysis [59-64]. With this in mind, though primarily

204 for economy, we regard PC 1 QTL as allometry QTL in the remainder of this manuscript.

205 The mouse subspecies that comprise the CC are estimated to have diverged several

206 hundred thousand years ago [65]. In many DO studies, subspecific divergence in one or more

207 wild-derived CC lines figures prominently in the founder genetic effects contrasts that underlie

208 QTL (e.g., [66-69]). Here, the same pattern is evident for most of the PC 1-4 QTL. In six of the

209 eight QTL (or seven of nine, if the two peaks of the PC 2, chromosome 14 QTL are considered

210 distinct), the coefficient for a non-*domesticus* wild-derived strain (CAST or PWK) sits at one
211 extreme of the founder coefficient distribution. Only at the upstream LOD peak of the PC 2,
212 chromosome 14 QTL is the founder coefficient contrast clearly between *M.m. domesticus*
213 inbred lines. The prevalence of QTL substantially driven by wild-derived alleles highlights the
214 value of subspecific genetic diversity in the DO population.

215 The broad region of high LOD scores for PC 1 on chromosome 7 merits individual
216 attention. This QTL support interval essentially delimits the mouse homolog boundaries of the
217 human Prader-Willi/Angelman syndromes domain [70]. The founder coefficients point to a
218 strong subspecies signal, with PWK (*M.m. musculus*) highly differentiated from wild-derived
219 WSB and the inbred *M.m. domesticus* lines, and CAST (*M.m. castaneus*) intermediate. Though
220 the QTL interval contains fewer than 40 genes, nine are known to be imprinted [70-74]. Several
221 more have mixed evidence for imprinting [73], and Prader-Willi and Angelman are parent-of-
222 origin dependent neurological disorders [75]. In addition, more than a dozen genes in the
223 interval are expressed in the developing face [40, 76-81]. Our mapping strategy is not
224 specifically designed to quantify imprinted gene QTL [82-84]. However, closer dissection of this
225 interval's contribution to facial shape variation, accounting for allelic parent of origin effects,
226 may be warranted in the future. The characteristic facial phenotype for Prader-Willi includes a
227 relatively long skull with a narrow upper face [85]. In this regard, the shape effects associated
228 with the peak marker in this interval, just downstream of the primary Prader-Willi genes, are
229 suggestive, as they contrast a shorter, wider face with a longer, narrower one (see **Figs 5 and 6**,
230 below).

231 **Marker Effects on Shape**

232 At the LOD peak marker of each PC 1-4 QTL, we collapsed the 8-state founder
233 probabilities to 2-state SNP probabilities in order to estimate the shape effect of allelic
234 substitution at that marker. To estimate effects on total shape (instead of univariate shape
235 PCs), we employed a Bayesian mixed effects model for highly multivariate dependent
236 observations [50, 86]. The results are plotted in **Fig 5**. In each figure, QTL effects are magnified
237 by the scaling factor required to cause the QTL to account for 10% of phenotypic variance.
238 These effects are shown as displacement vectors emanating from the mean configuration
239 wireframe. The magnification ensures that even when the effect at a landmark is small, its
240 direction and relative size (in comparison to effects at other landmarks) is apparent. We further
241 exploited the Bayesian posterior to plot 80% confidence ellipsoids for the magnified
242 displacements. The actual proportion of variance explained by the SNP, without magnification,
243 is noted in the figure (and included in **Table 3**).

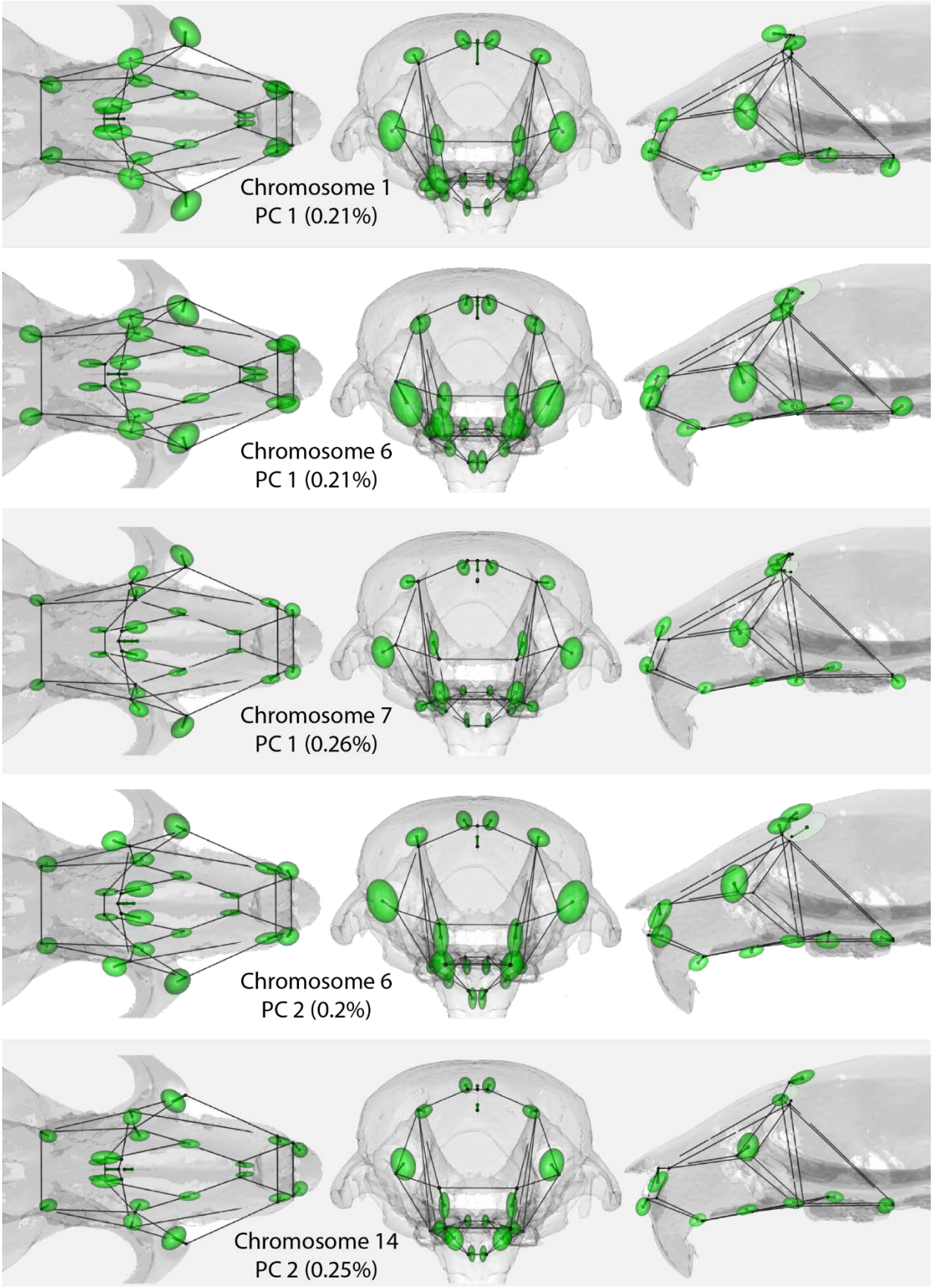
Chromosome 1
PC 1 (0.21%)
Chromosome 6
PC 1 (0.21%)
Chromosome 7
PC 1 (0.26%)
Chromosome 6
PC 2 (0.2%)
Chromosome 14
PC 2 (0.25%)

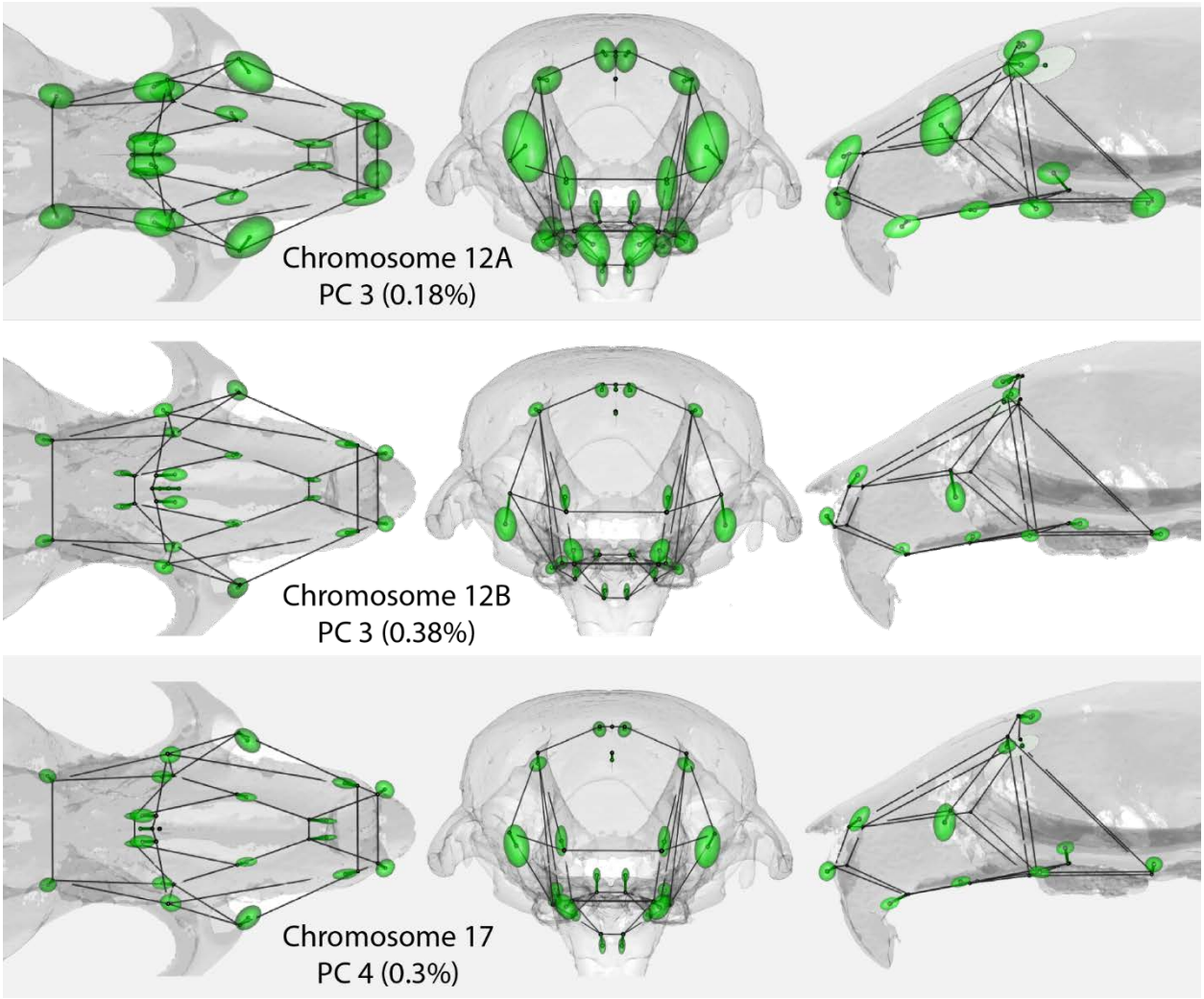

Fig 5. Superior (left), anterior (middle), and lateral (right) views of the (magnified) effect of allele substitution at the genome scan peak marker. Displacement vectors from wireframe to center of ellipsoids depict the mean effect. Ellipsoids enclose the approximate 80% posterior confidence boundaries.

Biological Process Enrichment

We used the human annotations in the online Molecular Signatures Database [87] to query biological processes relevant to craniofacial variation are overrepresented in the PC 1-4 QTL intervals. Collectively, the intervals contain 243 named, protein coding genes (**S1 File**), 232 of which are annotated in the Entrez Gene library utilized by the Molecular Signatures Database. **Table 2** provides GO biological process enrichment highlights for these intervals,

257 including FDR *q*-values adjusted for multiple testing (see **S2 File** for the top 100 *q*-value

258 processes). Growth, morphogenesis, and skeletal system development are prominent biological

259 process annotations for the facial shape QTL. The enrichment results suggest that no enriched

260 biological process is uniquely associated with shape variation on a single PC. Rather, with the

261 exception of bone development, each process in **Table 2** includes annotations to each PC.

262 **Table 2. Gene ontology enrichment for selected biological processes.**

Biological process	FDR *q* -value	GO annotated genes
Animal organ morphogenesis	1.42 e-3	**PC1:** *Aldh1a3, Chsy1, Nab1, Stat1, Trpm1.* **PC2:** *Col1a2, Dlg5, Gngt1, Hesx1, Tnnc1, Wnt5a, Zmiz1* . **PC3:** *Gdf7, Matn3, Osr1, Sdc1.* **PC4:** *Ccdc66, Mdfi, Ptk7, Runx2, Srf, Vegfa* .
Growth	2.25 e-3	**PC1:** *Apba2, Mstn, Ndn, Nsmce3, Ube3a* . **PC2:** *Bap1, Colq, Il17rb, Mustn1, Sema3g, Tkt, Wnt5a, Zmiz1.* **PC3:** *Gdf7, Matn3, Osr1* . **PC4:** *Dnph1, Mymx, Ptk7, Srf, Taf8, Vegfa, Hsp90ab1.*
Skeletal system development	1.29 e-2	**PC1:** *Chsy1, Nab1, Foxp1, Lrrk1.* **PC2:** *Col1a2, Mustn1, Wnt5a.* **PC3:** *Matn3, Osr1, Runx2.* **PC4:** *Mdfi, Srf.*
Sensory organ development	1.62 e-2	**PC1:** *Aldh1a3, Gabra5, Gabrb3, Trpm1.* **PC2:** *Ccdc66, Gngt1, Hesx1, Wnt5a.* **PC3:** *Osr1.* **PC4:** *Prph2, Ptk7, Srf, Vegfa.*
Cartilage development	2.4 e-2	**PC1:** *Chsy1.* **PC2:** *Mustn1, Wnt5a* . **PC3:** *Matn3, Osr1.* **PC4:** *Runx2, Srf.*
Bone development	2.54 e-2	**PC1:** *Chsy1, Nab1, Lrrk1, Foxp1.* **PC3:** *Matn3.* **PC4:** *Runx2, Srf* .

263

264 To consider annotations specific to allometric variation, we queried biological process

265 enrichment for PC 1 QTL alone (**S3 File**). Collectively, the three allometry QTL intervals were

266 significantly enriched for genes implicated in bone development (FDR q = 0.025). Each of the

267 intervals included at least one such gene: *Nab1* (chromosome 1) [88], *Foxp1* (chromosome 6)

268 [89, 90], and *Lrrk1* and *Chsy1* (chromosome 7) [91-93]. The chromosome 1 interval also includes

269 Myostatin (*Mstn, Gdf8*), a negative regulator of muscle growth. Inactivation of *Mstn* has been

270 shown to greatly increase facial muscle mass, with corresponding size decreases and shape

271 changes throughout the bony face and vault [94, 95].

272 **Association Mapping**

273 Finally, to develop a finer-grained impression of potential causal loci, we performed SNP

274 association mapping within each QTL interval. We imputed a dense map of SNP probabilities to

275 the sample by inferring their bi-allelic (major/minor) probabilities based on (a) founder

276 probabilities at flanking, genotyped markers and (b) major/minor strain distribution patterns in

277 the CC founder variants **(Fig 6)**.

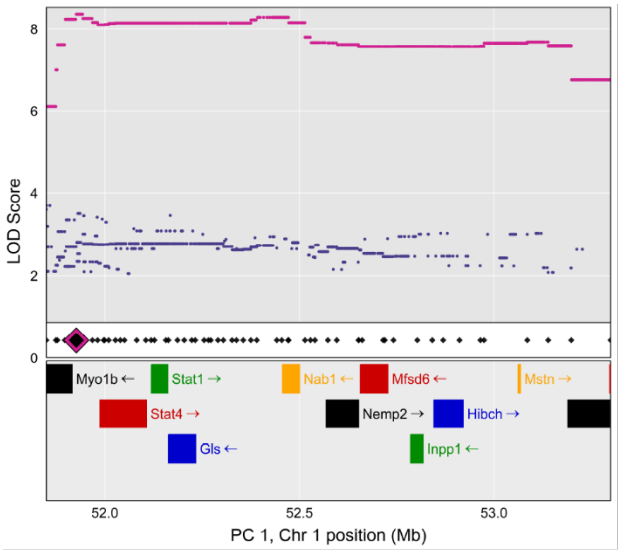
LOD Score
Myo1b
Stat1
Nab1
Mfsd6
Mstn
Stat4
Nemp2
Hibch
Gls
Inpp1
PC 1, Chr 1 position (Mb)

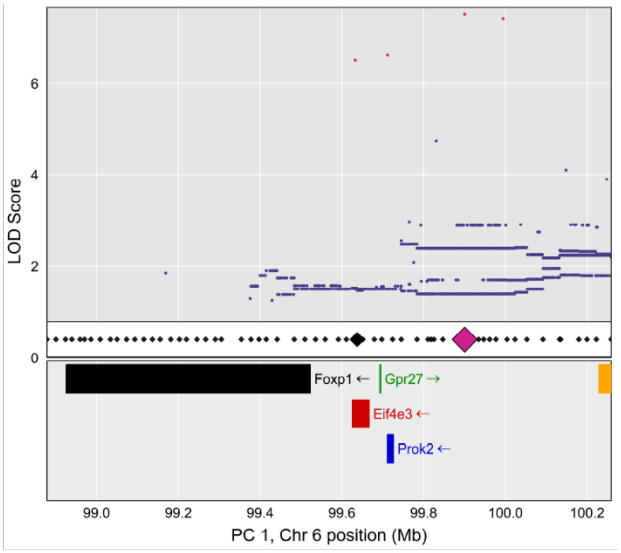
LOD Score
Foxp1
Gpr27
Eif4e3
Prok2
PC 1, Chr 6 position (Mb)

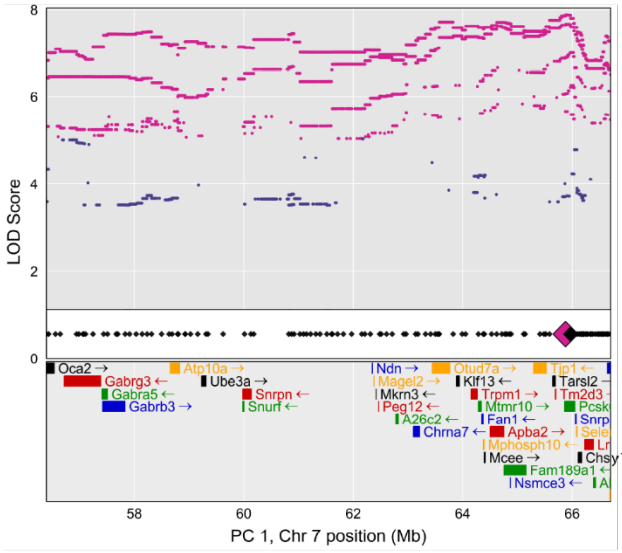
LOD Score
Oca2
Atp10a
Gabrg3
Ube3a
Gabra5
Snrpn
Gabrb3
Snurf
Ndn
Magel2
Klf13
Tarsl2
Mkrn3
Trpm1
Peg12
Mtmr10
A26c2
Fan1
Chrna7
Apba2
Mcee
Chsy1
Fam189a1
Nsmce3
PC 1, Chr 7 position (Mb)

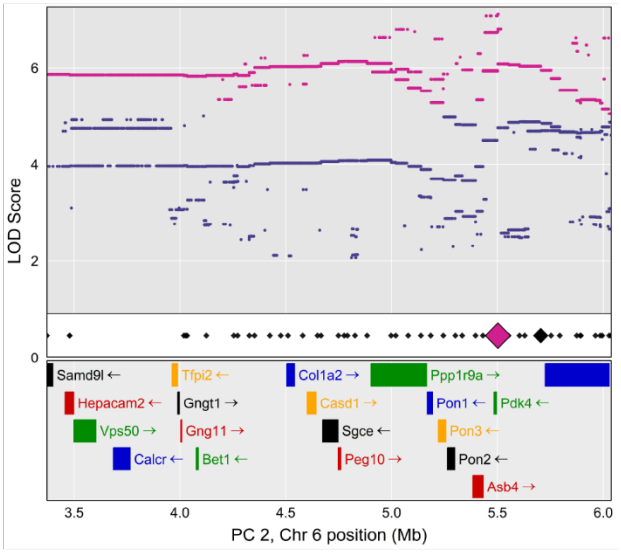
LOD Score
Samd9l
Tfpi2
Col1a2
Ppp1r9a
Hepacam2
Gngt1
Casd1
Pon1
Pdk4
Vps50
Gng11
Sgce
Pon3
Calcr
Bet1
Peg10
Pon2
Asb4
PC 2, Chr 6 position (Mb)

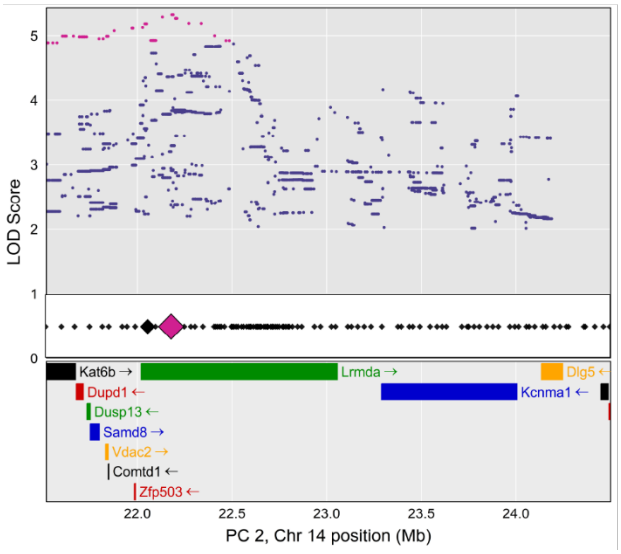
LOD Score
Kat6b
Lrmda
Dlg5
Dupd1
Kcnma1
Dusp13
Samd8
Vdac2
Comtd1
Zfp503
PC 2, Chr 14 position (Mb)

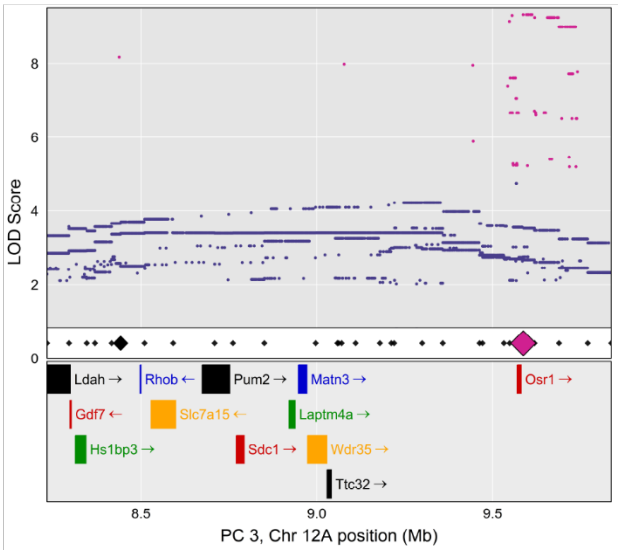
LOD Score
Ldah
Rhob
Pum2
Matn3
Osr1
Gdf7
Slc7a15
Laptm4a
Hs1bp3
Sdc1
Wdr35
Ttc32
PC 3, Chr 12A position (Mb)

278

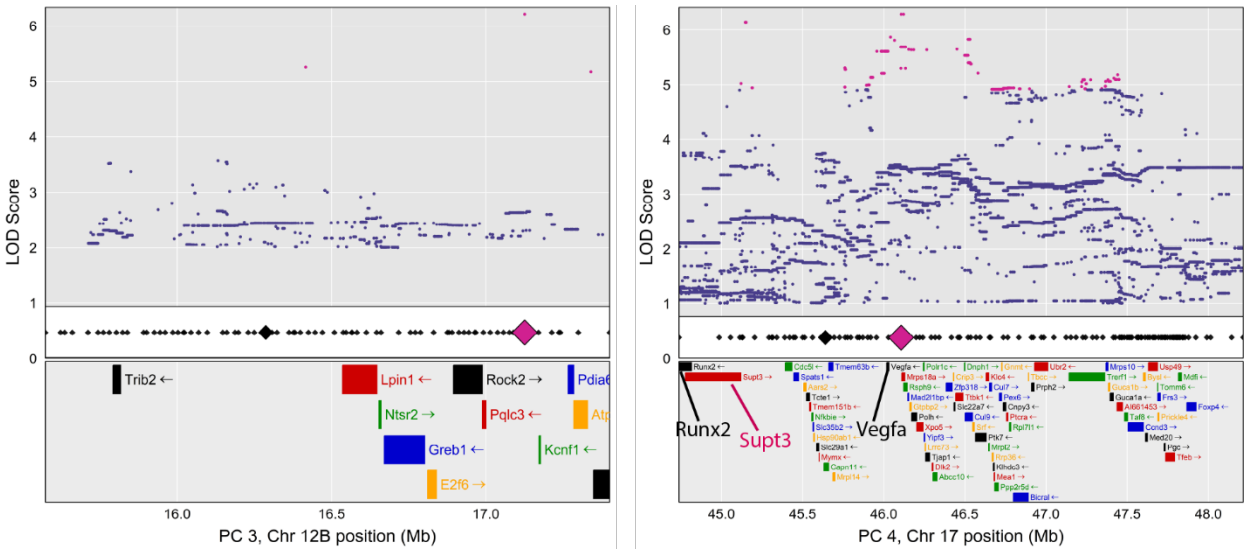

Fig 6. Association mapping results for PC 1-4 QTL intervals. Top panels: LOD scores for all CC SNP variants in the interval. Magenta points are locations where inferred bi-allelic SNP probabilities (based on strain distribution patterns in the CC) exceed the 95% LOD threshold. To control file size, low LOD scores points have been omitted from most plots. Middle panel: location of genotyped markers in the DO (small black diamonds), highlighting LOD peak locations for the founder genome scan (large black diamond) and SNP association scan (large magenta diamond). Bottom panel: named, protein coding genes for intervals. For legibility, we show the portion of the PC 2, Chromosome 14 map that contains both peak LOD scores and all SNPs exceeding the LOD threshold. For all plots, the complete gene list is provided in **S1 File**.

We then queried whether any genes within 0.25 Mb of the SNP or genome scan LOD peaks are known to be associated with craniofacial development or phenotypes **(Table 3)**. As with human facial shape GWAS [42], LOD peaks tended to be located in non-coding regions. While the focal genes we identified all have known roles in skeletal or craniofacial development, they also tend to be developmentally ubiquitous. *Stat1* (PC1, chr. 1) is implicated in bone development and remodeling throughout life [96-98]. Overexpression of *Foxp1* (PC1, chr. 6) can attenuate osteoblast differentiation, chondrocyte hypertrophy, osteoclastogenesis, and bone resorption, while *Foxp1* deficiency can accelerate ossification [89, 90]. In humans, some *Foxp1* mutations produce a facial phenotype that includes broad forehead and short nose

300 [99]. Chondrogenesis is generally disrupted in *Chsy1* null mouse mutants (PC1, chr. 7), and in
301 humans, *Chsy1* mutations can manifest in micrognathia and short stature [92, 100]. *Kat6b* (PC2,
302 Chr. 14) activates the transcription factor *Runx2*, which is often referred to as a master
303 regulator of bone formation [101-103]. For the PC3 QTL at 8.23 – 9.84 Mb on chromosome 12,
304 the founder and SNP LOD peaks reside at opposite ends of the QTL interval, but each is very
305 close to an important craniofacial development gene: *Gdf7* (*Bmp12*) contributes to patterning
306 of the jaw joint and is expressed in the developing incisor pulp and periodontium [104-106];
307 *Osr1* is broadly expressed in the embryonic and developing skull, with overexpression resulting
308 in intramembranous ossification deficiencies, increased chondrocyte differentiation, and
309 incomplete suture closure, while under-expression may contribute to cleft palate phenotype
310 [107-109]. *Osr1* has also previously been identified as a candidate in human facial shape GWAS
311 [23]. Finally, the SNP LOD peak for PC4, chromosome 17 implicates *Vegfa*, which is critical to
312 endochondral and intramembranous ossification through its role in angiogenesis [110]. A
313 distinct SNP LOD peak of nearly equal magnitude is located approximately 1 Mb upstream (at
314 rs47194347), very close to *Supt3* (human ortholog *Supt3h*) and *Runx2*. In addition to the central
315 role *Runx2* has in bone formation and development [102], both genes are human facial shape
316 GWAS candidates [15, 22].
317 **Table 3. Candidate genes.**

PC	Chr	Founder Peak (Mb)	Founder ID	Founder type	SNP Peak (Mb)	SNP ID	SNP_type	SNP % Var	Candidates
PC1	1	51.926616	rs48415864	intergenic	51.926623	rs254750887	intergenic	0.21	*STAT1*
PC1	6	99.637221	rs226005706	intron	99.900271	rs31234872	intergenic	0.21	*FOXP1*
PC1	7	65.970847	rs33905059	intron	65.876674	rs32405988	intron	0.26	*CHSY1*
PC2	6	5.704731	rs49620919	intergenic	5.502445	rs32485785	intergenic	0.2	NA
PC2	14	22.058402	rs30739483	intron	22.182166	rs30740474	intron	0.25	*KAT6B*
PC3	12	8.44203	rs48833407	intergenic	9.587123	rs29212735	intergenic	0.18	*OSR1, GDF7*
PC3	12	16.286802	rs49949506	intergenic	17.125642	SV 17121898: 17129386	structural (deletion)	0.38	NA
PC4	17	45.639772	rs107675960	intron	46.106749	rs108721614	upstream gene variant	0.3	*VEGFA [RUNX2, SUPT3]*

Candidate genes located within 0.25 Mb of founder or SNP QTL peaks. SNP % Var gives the percentage of variation explained by substitution of an additional reference allele at the founder (genome scan) peak.

While GP maps for traits influenced by many genes may be quite intricate and layered, additive effect QTL analyses remain an indispensable means to identify loci that contribute to phenotypic variation. Our investigation advances understanding of the genetics of facial skeletal diversity in several ways. The 37 QTL identified herein substantially expand the small but growing facial shape QTL library. Compared to similar prior studies, the number of QTL is relatively large and their confidence intervals relatively narrow. These results affirm the value of larger samples, sophisticated animal models like the outcrossed population utilized here, and high-resolution genotyping for identification and localization of QTL. Synthesizing our results with prior insights from developmental biology and medical genetics provides a richer picture of the sources of facial skeletal diversity. We found a relative abundance of skeletal and craniofacial development genes in QTL intervals for the largest shape PCs. Moreover, these genes tend to be located very close to QTL peaks. Thus, our results suggest that genes essential to building a face are often also the genes that cause faces to vary. Finally, QTL effect sizes were small. In summary, our results are consistent with a model of facial diversity that is influenced by key genes in skeletal and facial development and, simultaneously, highly polygenic.

338 ## Materials and methods

339 **Diversity Outbred mouse population**

340 The DO (Jackson Laboratory, www.jax.org) are derived from the eight inbred founder
341 lines that contribute to the CC [43, 44], which include three mouse subspecies, and both wild-
342 derived and laboratory strains [46]. Continued random outcrossing of the DO has produced a
343 population with relatively high genetic diversity (~45 million SNPs segregating in the CC
344 founding populations [43]) and increasingly fine mapping resolution in advancing generations.
345 In combination, these features increase the potential to identify multiple QTL for
346 complex traits [31]. On average, the genomes of the eight CC founders should be equally
347 represented in the DNA of any DO animal. Sequenced genomes for the CC make it possible to
348 characterize and interpret genetic variants in the DO according to 8-state founder identity and
349 as bi-allelic (major/minor allele) SNP variation. In addition, statistical packages designed for
350 analysis of the DO offer features to impute variants at each typed SNP in the CC founders, using
351 the coarser DO marker map as a scaffold to infer a high-density SNP map.

352 **Computing**

353 All analysis was conducted in R [111]. Customized data processing and statistical analysis
354 functions for mapping experiments in DO samples were originally published in the DOQTL
355 package [49]. These routines are now incorporated into the qlt2 package [48], with additional
356 processing and genotype diagnostic tools provided at https://kbroman.org/qtl2/.

357 **Images, landmark data**

358 Our DO sample consists of *n*=1147 male and female adult mice (after exclusion of some
359 records; see *Genotypes*, below) from seven DO generations (**Table 4**). No animals were

360 sacrificed for this study. Specimens were raised in several labs for unrelated experiments under
361 approval and conduced in accordance with the guidelines set forth by the Institutional Animal
362 Care and Use Committee in accordance with protocols #11-299 (University of North Carolina
363 Chapel Hill), #99066 and #15026 (Jackson Labs), and #08-0150-3 (Scripps Research Institute).
364 Receipt of animal carcasses and micro-CT (µCT) imaging of mouse skulls were undertaken in
365 accordance with approved IACUC protocol #AC18-0026 at the University of Calgary.

366 **Table 4. DO sample composition.**

	DO generation						
	9	**10**	**15**	**19**	**21**	**23**	**27**
Female	91	221	80	55	80	97	75
Male	0	144	0	58	77	99	70
MUGA Array	Mega	Mega	Mega	Giga	Giga	Giga	Giga

367
368 Overview of the DO sample by generation, sex, and genotyping array.
369
370 We obtained µCT images of the mouse skulls in the 3D Morphometrics Centre at the
371 University of Calgary on a Scanco vivaCT40 scanner (Scanco Medical, Brüttisellen, Switzerland)
372 at 0.035 mm voxel dimensions at 55kV and 72-145 µA. On each skull, one of us (WL) collected
373 54 3D landmark coordinates from minimum threshold-defined bone surface with ANALYZE 3D
374 (www.mayo.edu/bir/). Here, we analyzed the 22-landmark subset of the full configuration—a
375 66 coordinate dimension vector—that captures the shape of the face (**Fig 1**).

376 **Shape data**

377 Landmark configurations were symmetrically superimposed by Generalized Procrustes
378 Analysis (GPA) [112] using the Morpho package [113]. GPA is a multi-step procedure that
379 removes location and centroid size differences between configurations, then (iteratively)
380 rotates each configuration to minimize its squared distance from the sample mean. We chose a
381 superimposition that decomposes shape variation into its symmetric and asymmetric

382 components [114, 115], and stored the symmetric configurations for analysis. Working with
383 symmetric, superimposed data reduced morphological degrees of freedom from 66 landmark
384 coordinate dimensions to 30 shape dimensions [115].

385 **Genotypes**

386 For all animals, DNA was extracted from ear or tail clippings. Genotyping was performed
387 by the Geneseek operations of Neogen Corp. (Lincoln, NE). Mice from generations 9, 10, and 15
388 were genotyped using the MegaMUGA genotyping array (77,808 markers); mice from
389 generations 19, 21, 23, and 27 were genotyped using the larger GigaMUGA array (143,259
390 markers) [116]. The two arrays share 58,907 markers in common. We restricted the genotype
391 data to these shared SNPs [116].

392 In addition, we excluded 2,022 markers from the center of chromosome 2 (40 - 140
393 Mb). WSB alleles are highly overrepresented in this genomic region in earlier DO generations.
394 This overrepresentation has been attributed to female meiotic drive favoring WSB at the *R2d2*
395 locus [117]. Between DO generations 12 and 21, Jackson Labs systematically purged the meiotic
396 drive locus and linked effects from the DO [45]. Our samples closely track this history, with WSB
397 allele frequencies in the middle of chromosome 2 exceeding 60% in generation 9 and falling to
398 0% by generation 23 (**S2 Fig**). If unaddressed, this directional shift in allele frequencies can
399 confound statistical analysis of genotype-phenotype associations [118] with potentially false
400 positive associations between WSB chromosome 2 haplotypes and directional changes in
401 phenotype over DO generations. After removing this genomic region from consideration, the
402 final SNP dataset consists of 56,885 markers common to the MegaMUGA and GigaMUGA
403 arrays, with a mean spacing of 48 kb.

404 The qtl2 package estimates genotype probabilities, including imputation of sporadically
405 missing genotypes, with a multipoint Hidden Markov Model (HMM) on the observed marker
406 genotypes. From these initial genotype probabilities, we derived three probabilistic
407 representations of genetic state for each observation at each marker: (1) for genome scans,
408 founder probabilities, a vector encoding the probability of genetic contribution from each of
409 the eight CC founders to the diplotype state; (2) for association mapping, SNP probabilities,
410 collapsing the eight founder probabilities to a two-state, major/minor allele strain distribution;
411 and (3) for mapping multivariate shape effects, additive SNP dosage, twice the estimated major
412 SNP probability (maximum additive SNP dosage = 2).
413 We identified problematic genetic samples using the DO genotype diagnostics tools
414 available at https://kbroman.org/qtl2/ [119]. A total of 11 observations were excluded due to
415 excessive missing marker data, which we defined as no marker information at >7.5% of
416 markers. Three probable duplicate sets of genetic data (>99% of markers identical) were
417 identified. Because the correct genotype-phenotype matches could not be established by other
418 evidence, all six animals were removed from the sample. Finally, we excluded seven female
419 samples with low X chromosome array intensity values. These samples are potentially XO [45],
420 which can affect facial form and body size [120, 121]. The exclusions described above resulted
421 in a final, retained sample of n = 1147 animals.
422 **Genome scan and association mapping**
423 We mapped QTL for facial shape and facial shape allometry. To identify QTL, we
424 implemented the linear mixed effects regression model in qtl2. The qtl2 genome scan is
425 designed to estimate marker effects on one or more univariate observations, but not

426 covariance among those dimensions. We therefore decomposed the superimposed coordinates
427 into PCs, treating the specimen scores on each PC as measured traits. For allometry, we treated
428 common allometric component scores [61] as measured traits. Prior to deriving PCs and
429 allometry vectors, we centered each observation on its generation mean in order to focus on
430 shared, within-generation covariance patterns [122, p. 295].

431 At each marker, we fit a mixed model with fixed effect coefficients for sex, age-at-
432 sacrifice, and the additive effect of each CC founder haplotype, a random effect of kinship, and
433 an error term [49]. Evidence for a QTL was evaluated based on marker LOD scores, likelihood
434 ratios comparing the residuals of the marker model to a null model excluding the marker's
435 effect [51]. We consider the evidence for a marker-phenotype association to be statistically
436 significant where the LOD score exceeds the 95% quantile of genome-wide maximum LOD
437 scores computed from 1000 random permutations of genotype-phenotype associations [123].
438 We use a 1.5 LOD-drop rule to define the boundaries of QTL support intervals [124], and allow
439 for multiple QTL peaks on a single chromosome.

440 The random effect of kinship depends upon pairwise proportions of shared alleles
441 among observations, encoded in a kinship matrix. Loss of power to detect QTL can arise when
442 the marker of interest and linked genes are included in the kinship matrix of the null model. To
443 avoid this problem, we compute kinship matrices using a leave-one-chromosome-out (LOCO)
444 approach [52-54].

445 Genome scans, QTL support intervals, and proportions of shape variation attributable to
446 founder-level kinship (heritability) were estimated for all PCs explaining more than 1% of
447 symmetric shape variation. However, we limit more in-depth analysis to the five PCs with

448 reasonably large signal-to-noise ratios (**S2 Fig**). This was assessed using the modified "noise
449 floor" detection strategy developed by Marroig and colleagues in [56].
450 In addition, within the PC 1-5 QTL intervals, we used a form of merge analysis to
451 perform genome-wide association mapping [49, 125, 126]. For each CC founder variant located
452 between a flanking pair of genotyped markers, the vector of founder allele probabilities is
453 assumed to be the average of the founder probabilities at those flanking markers. The bi-allelic
454 SNP probabilities were computed from these founder probabilities and the major/minor allele
455 strain distribution pattern in the CC. Analysis was again via mixed effects regression model, with
456 the imputed SNP data as genotype predictors.
457 **Enrichment analysis and candidate genes**
458 Modern GWAS and QTL studies often attempt to contextualize QTL and candidate gene
459 results post hoc via GO enrichment analysis. Given a list of genes near statistically significant
460 markers, a GO analysis calculates the probability that a random set of genes of the same size
461 would contain as many genes under a common annotation term, typically after a family-wise
462 error rate or FDR adjustment for multiple testing. The outcome of enrichment analysis is a list
463 of GO terms (or in the absence of any enrichment, no list), which provides a means to consider
464 whether certain biological processes, cellular components, or molecular functions are over-
465 represented in the list of genes [127].
466 For protein coding genes in the PC 1-5 QTL support intervals and for allometry QTL, we
467 used the Molecular Signatures Database [87] online tool and Entrez Gene library [128] to
468 identify biological process GO term enrichment [129]. The database application implements a
469 hypergeometric test of statistical significance, quantifying the probability of sampling, without

470 replacement, as many (*k*) or more genes annotated to a GO term, given the total number of
471 genes annotated to that term (*K*) and the number of genes in the QTL and Entrez gene sets (*n*
472 and *N,* respectively). For each ontology term, after adjustment for multiple testing, we required
473 a FDR *q*-value < 0.05 to conclude that there was substantial evidence for GO biological process
474 enrichment. We also inspected the association mapping results in the +/- 0.25 Mb region
475 centered at each LOD peak for genes with convincing evidence of a role in skeletal, craniofacial,
476 or dental development or disease. For most QTL, LOD peaks for the genome scan and
477 association mapping results are virtually coincident. Where they differ substantially, we
478 examine the region around both peaks.

479 **Marker effects on shape**

480 We considered a significant association between a marker and facial shape along a PC
481 axis to be evidence of some effect on the multivariate (undecomposed) shape coordinate data.
482 In order to obtain an estimate of the full shape effect, we fit an additional mixed model for the
483 maximum LOD score marker. Fitting a mixed model for highly multivariate data presents a
484 significant computational challenge because the number of parameters that must be estimated
485 for the random effects covariance matrix scales quadratically with the number of traits (here,
486 465 parameters for 30 free variables). To address this challenge, we estimated mixed model
487 covariance matrices using a Bayesian sparse factorization approach [50, 86, 130]. After a
488 1,000,000 iteration burn-in, we generated 1,000,000 realizations from a single Markov chain,
489 thinning at a rate of 1,000 to store 1,000 posterior samples for inference. Though the time
490 needed to fit such a model makes it impractical for a genome scan on a dense array, it is a
491 useful strategy for disentangling kinship from the effect on multivariate outcomes at a small

492 number of peak markers. For these regressions, the marker effect predictor was twice the
493 major SNP probability. Thus, the multivariate mixed model we implemented estimates an
494 average effect of allele substitution, a standard quantity in quantitative genetics [131]. In
495 addition, for each regression, we estimated the proportion of shape variation explained using a
496 version of the coefficient of determination (R^2) that has been adapted for mixed model
497 parameters [132].

498 When plotting shape effects, we magnify the allele substitution coefficients by the
499 scaling factor needed to cause the QTL to explain 5% of phenotypic variance. This magnification
500 is applied both to the mean effect, in order to depict the mean displacement vector, and to the
501 posterior distribution of effects, in order to depict confidence ellipsoids. Ellipsoids were
502 estimated with the 3D ellipse function in the R package rgl [133]. While it is more typical to use
503 a 95% support boundary to evaluate effect uncertainty, with shape data, morphological
504 contrasts are best understood over the configuration as a whole [134]. The 80% ellipsoids are
505 meant to encourage this perspective.

506

507 **Acknowledgements**

508 Thanks to Xiang Zhao for help with preparation of samples and David Eby for helpful
509 intervention with the online Molecular Signatures Database. We thank Kunjie Hua, Liyang Zhao
510 and Kuo-Chen Jung for assistance with UNC mouse experiments. Charles Farber is gratefully
511 acknowledged for assistance with processing of UNC mouse carcasses. All UNC mouse
512 procedures were approved and guided by the appropriate institutional animal ethics
513 committees, including the University of North Carolina at Chapel Hill.

REFERENCES

1. Hu D, Marcucio RS. A SHH-responsive signaling center in the forebrain regulates craniofacial morphogenesis via the facial ectoderm. Development. 2009;136(1):107-16. Epub 2008/11/26. doi: 10.1242/dev.026583. PubMed PMID: 19036802; PubMed Central PMCID: PMCPMC2685963.
2. Hallgrímsson B, Jamniczky H, Young NM, Rolian C, Parsons TE, Boughner JC, et al. Deciphering the palimpsest: studying the relationship between morphological integration and phenotypic covariation. Evolutionary Biology. 2009;36(4):355-76.
3. Hallgrimsson B, Mio W, Marcucio RS, Spritz R. Let's face it--complex traits are just not that simple. PLoS Genet. 2014;10(11):e1004724. Epub 2014/11/06. doi: 10.1371/journal.pgen.1004724. PubMed PMID: 25375250; PubMed Central PMCID: PMCPMC4222688.
4. Varón-González C, Pallares LF, Debat V, Navarro N. Mouse Skull Mean Shape and Shape Robustness Rely on Different Genetic Architectures and Different Loci. Front Genet. 2019;10:64. Epub 2019/02/12. doi: 10.3389/fgene.2019.00064. PubMed PMID: 30809244; PubMed Central PMCID: PMCPMC6379267.
5. Young NM, Chong HJ, Hu D, Hallgrímsson B, Marcucio RS. Quantitative analyses link modulation of sonic hedgehog signaling to continuous variation in facial growth and shape. Development. 2010;137(20):3405-9. Epub 2010/09/08. doi: 10.1242/dev.052340. PubMed PMID: 20826528; PubMed Central PMCID: PMCPMC2947484.
6. Green RM, Fish JL, Young NM, Smith FJ, Roberts B, Dolan K, et al. Developmental nonlinearity drives phenotypic robustness. Nat Commun. 2017;8(1):1970. Epub 2017/12/06. doi: 10.1038/s41467-017-02037-7. PubMed PMID: 29213092; PubMed Central PMCID: PMCPMC5719035.
7. Mitteroecker P, Bookstein F. The Conceptual and Statistical Relationship between Modularity and Morphological Integration. Systematic Biology. 2007;56(5):818-36. doi: 10.1080/10635150701648029.
8. Szabo-Rogers HL, Smithers LE, Yakob W, Liu KJ. New directions in craniofacial morphogenesis. Dev Biol. 2010;341(1):84-94. Epub 2009/11/24. doi: 10.1016/j.ydbio.2009.11.021. PubMed PMID: 19941846.
9. Francis-West P, Crespo-Enriquez I. Vertebrate Embryo: Craniofacial Development. eLS [Internet]. 2016:[1-15 pp.].
10. Falconer DS, Mackay TF. Introduction to quantitative genetics. 4th ed. Essex: Pearson Education Limited; 2009.
11. Huang W, Mackay TF. The Genetic Architecture of Quantitative Traits Cannot Be Inferred from Variance Component Analysis. PLoS Genet. 2016;12(11):e1006421. Epub 2016/11/03. doi: 10.1371/journal.pgen.1006421. PubMed PMID: 27812106; PubMed Central PMCID: PMCPMC5094750.
12. Barton NH, Keightley PD. Understanding quantitative genetic variation. Nat Rev Genet. 2002;3(1):11-21. doi: 10.1038/nrg700. PubMed PMID: 11823787.

555 13. Varón-González C, Navarro N. Epistasis regulates the developmental stability of the
556 mouse craniofacial shape. Heredity (Edinb). 2019;122(5):501-12. Epub 2018/09/12. doi:
557 10.1038/s41437-018-0140-8. PubMed PMID: 30209292; PubMed Central PMCID:
558 PMCPMC6461946.
559 14. Wolf JB, Leamy LJ, Routman EJ, Cheverud JM. Epistatic pleiotropy and the genetic
560 architecture of covariation within early and late-developing skull trait complexes in mice.
561 Genetics. 2005;171(2):683-94. Epub 2005/07/14. doi: 10.1534/genetics.104.038885. PubMed
562 PMID: 16020793; PubMed Central PMCID: PMCPMC1456798.
563 15. Claes P, Roosenboom J, White JD, Swigut T, Sero D, Li J, et al. Genome-wide mapping of
564 global-to-local genetic effects on human facial shape. Nat Genet. 2018;50(3):414-23. Epub
565 2018/02/19. doi: 10.1038/s41588-018-0057-4. PubMed PMID: 29459680; PubMed Central
566 PMCID: PMCPMC5937280.
567 16. Lee MK, Shaffer JR, Leslie EJ, Orlova E, Carlson JC, Feingold E, et al. Genome-wide
568 association study of facial morphology reveals novel associations with FREM1 and PARK2. PLoS
569 One. 2017;12(4):e0176566. Epub 2017/04/25. doi: 10.1371/journal.pone.0176566. PubMed
570 PMID: 28441456; PubMed Central PMCID: PMCPMC5404842.
571 17. Liu F, van der Lijn F, Schurmann C, Zhu G, Chakravarty MM, Hysi PG, et al. A genome-
572 wide association study identifies five loci influencing facial morphology in Europeans. PLoS
573 Genet. 2012;8(9):e1002932. Epub 2012/09/13. doi: 10.1371/journal.pgen.1002932. PubMed
574 PMID: 23028347; PubMed Central PMCID: PMCPMC3441666.
575 18. Paternoster L, Zhurov AI, Toma AM, Kemp JP, St Pourcain B, Timpson NJ, et al. Genome-
576 wide association study of three-dimensional facial morphology identifies a variant in PAX3
577 associated with nasion position. Am J Hum Genet. 2012;90(3):478-85. Epub 2012/02/16. doi:
578 10.1016/j.ajhg.2011.12.021. PubMed PMID: 22341974; PubMed Central PMCID:
579 PMCPMC3309180.
580 19. Shaffer JR, Orlova E, Lee MK, Leslie EJ, Raffensperger ZD, Heike CL, et al. Genome-Wide
581 Association Study Reveals Multiple Loci Influencing Normal Human Facial Morphology. PLoS
582 Genet. 2016;12(8):e1006149. Epub 2016/08/25. doi: 10.1371/journal.pgen.1006149. PubMed
583 PMID: 27560520; PubMed Central PMCID: PMCPMC4999139.
584 20. Crouch DJM, Winney B, Koppen WP, Christmas WJ, Hutnik K, Day T, et al. Genetics of the
585 human face: Identification of large-effect single gene variants. Proc Natl Acad Sci U S A.
586 2018;115(4):E676-E85. Epub 2018/01/04. doi: 10.1073/pnas.1708207114. PubMed PMID:
587 29301965; PubMed Central PMCID: PMCPMC5789906.
588 21. Cole JB, Manyama M, Kimwaga E, Mathayo J, Larson JR, Liberton DK, et al. Genomewide
589 Association Study of African Children Identifies Association of SCHIP1 and PDE8A with Facial
590 Size and Shape. PLoS Genet. 2016;12(8):e1006174. Epub 2016/08/25. doi:
591 10.1371/journal.pgen.1006174. PubMed PMID: 27560698; PubMed Central PMCID:
592 PMCPMC4999243.
593 22. Adhikari K, Fuentes-Guajardo M, Quinto-Sánchez M, Mendoza-Revilla J, Camilo Chacón-
594 Duque J, Acuña-Alonzo V, et al. A genome-wide association scan implicates DCHS2, RUNX2,
595 GLI3, PAX1 and EDAR in human facial variation. Nat Commun. 2016;7:11616. Epub 2016/05/19.
596 doi: 10.1038/ncomms11616. PubMed PMID: 27193062; PubMed Central PMCID:
597 PMCPMC4874031.

598 23. Cha S, Lim JE, Park AY, Do JH, Lee SW, Shin C, et al. Identification of five novel genetic
599 loci related to facial morphology by genome-wide association studies. BMC Genomics.
600 2018;19(1):481. Epub 2018/06/19. doi: 10.1186/s12864-018-4865-9. PubMed PMID: 29921221;
601 PubMed Central PMCID: PMCPMC6008943.
602 24. Richmond S, Howe LJ, Lewis S, Stergiakouli E, Zhurov A. Facial Genetics: A Brief
603 Overview. Front Genet. 2018;9:462. Epub 2018/10/16. doi: 10.3389/fgene.2018.00462.
604 PubMed PMID: 30386375; PubMed Central PMCID: PMCPMC6198798.
605 25. Cole J, Spritz RA. The genetics of facial morphology. eLS [Internet]. 2017:[1-9 pp.].
606 26. Cheverud JM, Routman EJ, Irschick DJ. PLEIOTROPIC EFFECTS OF INDIVIDUAL GENE LOCI
607 ON MANDIBULAR MORPHOLOGY. Evolution. 1997;51(6):2006-16. doi: 10.1111/j.1558-
608 5646.1997.tb05122.x. PubMed PMID: 28565113.
609 27. Kenney-Hunt JP, Wang B, Norgard EA, Fawcett G, Falk D, Pletscher LS, et al. Pleiotropic
610 patterns of quantitative trait loci for 70 murine skeletal traits. Genetics. 2008;178(4):2275-88.
611 doi: 10.1534/genetics.107.084434. PubMed PMID: 18430949; PubMed Central PMCID:
612 PMCPMC2323815.
613 28. Pallares LF, Harr B, Turner LM, Tautz D. Use of a natural hybrid zone for genomewide
614 association mapping of craniofacial traits in the house mouse. Mol Ecol. 2014;23(23):5756-70.
615 Epub 2014/11/15. doi: 10.1111/mec.12968. PubMed PMID: 25319559.
616 29. Klingenberg CP, Leamy LJ. Quantitative genetics of geometric shape in the mouse
617 mandible. Evolution. 2001;55(11):2342-52. doi: 10.1111/j.0014-3820.2001.tb00747.x.
618 30. Klingenberg CP, Leamy LJ, Cheverud JM. Integration and Modularity of Quantitative Trait
619 Locus Effects on Geometric Shape in the Mouse Mandible. Genetics. 2004;166(4):1909-21. doi:
620 10.1534/genetics.166.4.1909.
621 31. Flint J, Eskin E. Genome-wide association studies in mice. Nat Rev Genet.
622 2012;13(11):807-17. Epub 2012/10/09. doi: 10.1038/nrg3335. PubMed PMID: 23044826;
623 PubMed Central PMCID: PMCPMC3625632.
624 32. Pallares LF, Carbonetto P, Gopalakrishnan S, Parker CC, Ackert-Bicknell CL, Palmer AA, et
625 al. Mapping of Craniofacial Traits in Outbred Mice Identifies Major Developmental Genes
626 Involved in Shape Determination. PLoS Genet. 2015;11(11):e1005607. Epub 2015/11/02. doi:
627 10.1371/journal.pgen.1005607. PubMed PMID: 26523602; PubMed Central PMCID:
628 PMCPMC4629907.
629 33. Maga AM, Navarro N, Cunningham ML, Cox TC. Quantitative trait loci affecting the 3D
630 skull shape and size in mouse and prioritization of candidate genes in-silico. Front Physiol.
631 2015;6:92. Epub 2015/03/26. doi: 10.3389/fphys.2015.00092. PubMed PMID: 25859222;
632 PubMed Central PMCID: PMCPMC4374467.
633 34. Percival CJ, Green R, Roseman CC, Gatti DM, Morgan JL, Murray SA, et al.
634 Developmental constraint through negative pleiotropy in the zygomatic arch. Evodevo.
635 2018;9:3. Epub 2018/01/27. doi: 10.1186/s13227-018-0092-3. PubMed PMID: 29423138;
636 PubMed Central PMCID: PMCPMC5787316.
637 35. Gudbjartsson DF, Walters GB, Thorleifsson G, Stefansson H, Halldorsson BV,
638 Zusmanovich P, et al. Many sequence variants affecting diversity of adult human height. Nat
639 Genet. 2008;40(5):609-15. Epub 2008/04/06. doi: 10.1038/ng.122. PubMed PMID: 18391951.
640 36. Cole J, Manyama M, Larson JR, Liberton DK, Ferrara TM, Riccardi SL, et al. Human Facial
641 Shape and Size Heritability and Genetic Correlations. Genetics. 2017;205(2):967-78. Epub

642 2016/12/14. doi: 10.1534/genetics.116.193185. PubMed PMID: 27974501; PubMed Central
643 PMCID: PMCPMC5289863.
644 37. de Los Campos G, Vazquez AI, Hsu S, Lello L. Complex-Trait Prediction in the Era of Big
645 Data. Trends Genet. 2018;34(10):746-54. Epub 2018/08/20. doi: 10.1016/j.tig.2018.07.004.
646 PubMed PMID: 30139641; PubMed Central PMCID: PMCPMC6150788.
647 38. Wilderman A, VanOudenhove J, Kron J, Noonan JP, Cotney J. High-Resolution
648 Epigenomic Atlas of Human Embryonic Craniofacial Development. Cell Rep. 2018;23(5):1581-
649 97. doi: 10.1016/j.celrep.2018.03.129. PubMed PMID: 29719267; PubMed Central PMCID:
650 PMCPMC5965702.
651 39. Hooper JE, Feng W, Li H, Leach SM, Phang T, Siska C, et al. Systems biology of facial
652 development: contributions of ectoderm and mesenchyme. Dev Biol. 2017;426(1):97-114. Epub
653 2017/03/29. doi: 10.1016/j.ydbio.2017.03.025. PubMed PMID: 28363736; PubMed Central
654 PMCID: PMCPMC5530582.
655 40. Diez-Roux G, Banfi S, Sultan M, Geffers L, Anand S, Rozado D, et al. A high-resolution
656 anatomical atlas of the transcriptome in the mouse embryo. PLoS Biol. 2011;9(1):e1000582.
657 Epub 2011/01/18. doi: 10.1371/journal.pbio.1000582. PubMed PMID: 21267068; PubMed
658 Central PMCID: PMCPMC3022534.
659 41. Mackay TFC, Stone EA, Ayroles JF. The genetics of quantitative traits: challenges and
660 prospects. Nat Rev Genet. 2009;10(8):565-77. doi:
661 http://www.nature.com/nrg/journal/v10/n8/suppinfo/nrg2612_S1.html.
662 42. Weinberg SM, Roosenboom J, Shaffer JR, Shriver MD, Wysocka J, Claes P. Hunting for
663 genes that shape human faces: Initial successes and challenges for the future. Orthod Craniofac
664 Res. 2019;22 Suppl 1:207-12. doi: 10.1111/ocr.12268. PubMed PMID: 31074157; PubMed
665 Central PMCID: PMCPMC6550302.
666 43. Svenson KL, Gatti DM, Valdar W, Welsh CE, Cheng R, Chesler EJ, et al. High-resolution
667 genetic mapping using the Mouse Diversity outbred population. Genetics. 2012;190(2):437-47.
668 doi: 10.1534/genetics.111.132597. PubMed PMID: 22345611; PubMed Central PMCID:
669 PMCPMC3276626.
670 44. Churchill GA, Gatti DM, Munger SC, Svenson KL. The Diversity Outbred mouse
671 population. Mamm Genome. 2012;23(9-10):713-8. Epub 2012/08/15. doi: 10.1007/s00335-012-
672 9414-2. PubMed PMID: 22892839; PubMed Central PMCID: PMCPMC3524832.
673 45. Chesler EJ, Gatti DM, Morgan AP, Strobel M, Trepanier L, Oberbeck D, et al. Diversity
674 Outbred Mice at 21: Maintaining Allelic Variation in the Face of Selection. G3 (Bethesda).
675 2016;6(12):3893-902. Epub 2016/12/07. doi: 10.1534/g3.116.035527. PubMed PMID:
676 27694113; PubMed Central PMCID: PMCPMC5144960.
677 46. Yang H, Wang JR, Didion JP, Buus RJ, Bell TA, Welsh CE, et al. Subspecific origin and
678 haplotype diversity in the laboratory mouse. Nat Genet. 2011;43(7):648-55. Epub 2011/05/29.
679 doi: 10.1038/ng.847. PubMed PMID: 21623374; PubMed Central PMCID: PMCPMC3125408.
680 47. Consortium CC. The genome architecture of the Collaborative Cross mouse genetic
681 reference population. Genetics. 2012;190(2):389-401. doi: 10.1534/genetics.111.132639.
682 PubMed PMID: 22345608; PubMed Central PMCID: PMCPMC3276630.
683 48. Broman KW, Gatti DM, Simecek P, Furlotte NA, Prins P, Sen Ś, et al. R/qtl2: Software for
684 Mapping Quantitative Trait Loci with High-Dimensional Data and Multiparent Populations.

685 Genetics. 2019;211(2):495-502. Epub 2018/12/27. doi: 10.1534/genetics.118.301595. PubMed
686 PMID: 30591514; PubMed Central PMCID: PMCPMC6366910.
687 49. Gatti DM, Svenson KL, Shabalin A, Wu LY, Valdar W, Simecek P, et al. Quantitative trait
688 locus mapping methods for diversity outbred mice. G3 (Bethesda). 2014;4(9):1623-33. Epub
689 2014/09/18. doi: 10.1534/g3.114.013748. PubMed PMID: 25237114; PubMed Central PMCID:
690 PMCPMC4169154.
691 50. Runcie DE, Mukherjee S. Dissecting High-Dimensional Phenotypes with Bayesian Sparse
692 Factor Analysis of Genetic Covariance Matrices. Genetics. 2013;194(3):753-67. doi:
693 10.1534/genetics.113.151217.
694 51. Lander ES, Botstein D. Mapping mendelian factors underlying quantitative traits using
695 RFLP linkage maps. Genetics. 1989;121(1):185-99. PubMed PMID: 2563713; PubMed Central
696 PMCID: PMCPMC1203601.
697 52. Listgarten J, Lippert C, Kadie CM, Davidson RI, Eskin E, Heckerman D. Improved linear
698 mixed models for genome-wide association studies. Nat Methods. 2012;9(6):525-6. Epub
699 2012/05/30. doi: 10.1038/nmeth.2037. PubMed PMID: 22669648; PubMed Central PMCID:
700 PMCPMC3597090.
701 53. Cheng R, Parker CC, Abney M, Palmer AA. Practical considerations regarding the use of
702 genotype and pedigree data to model relatedness in the context of genome-wide association
703 studies. G3 (Bethesda). 2013;3(10):1861-7. Epub 2013/10/03. doi: 10.1534/g3.113.007948.
704 PubMed PMID: 23979941; PubMed Central PMCID: PMCPMC3789811.
705 54. Yang J, Zaitlen NA, Goddard ME, Visscher PM, Price AL. Advantages and pitfalls in the
706 application of mixed-model association methods. Nat Genet. 2014;46(2):100-6. doi:
707 10.1038/ng.2876. PubMed PMID: 24473328; PubMed Central PMCID: PMCPMC3989144.
708 55. Tsagkrasoulis D, Hysi P, Spector T, Montana G. Heritability maps of human face
709 morphology through large-scale automated three-dimensional phenotyping. Sci Rep.
710 2017;7:45885. Epub 2017/04/19. doi: 10.1038/srep45885. PubMed PMID: 28422179; PubMed
711 Central PMCID: PMCPMC5395823.
712 56. Marroig G, Melo DA, Garcia G. Modularity, noise, and natural selection. Evolution.
713 2012;66(5):1506-24.
714 57. Mrode RA. Linear models for the prediction of animal breeding values. 3rd ed.
715 Oxfordshire, UK: CABI; 2014.
716 58. Robinson GK. That BLUP is a good thing: the estimation of random effects. Statistical
717 Science. 1991;6(1):15-51. doi: 10.1214/ss/1177011933.
718 59. Hallgrimsson B, Katz DC, Aponte JD, Larson JE, Devine J, Gonzalez P, et al. Integration
719 and the developmental genetics of allometry. Integrative and Comparative Biology. 2019, in
720 press.
721 60. Jolicoeur P, Mosimann JE. Size and shape variation in the painted turtle. A principal
722 component analysis. Growth. 1960;24:339-54. PubMed PMID: 13790416.
723 61. Mitteroecker P, Gunz P, Bernhard M, Schaefer K, Bookstein F. Comparison of cranial
724 ontogenetic trajectories among great apes and humans. Journal of Human Evolution.
725 2004;46(6):679-98. doi: 10.1016/j.jhevol.2004.03.006.
726 62. Mosimann JE. Size allometry: Size and shape variables with characterizations of the
727 lognormal and generalized gamma distributions. Journal of the American Statistical Association.
728 1970;65:930-45.

63. Cheverud JM. Relationships among ontogenetic, static, and evolutionary allometry. Am J Phys Anthropol. 1982;59(2):139-49. doi: 10.1002/ajpa.1330590204. PubMed PMID: 7149015.
64. Larson JR, Manyama MF, Cole JB, Gonzalez PN, Percival CJ, Liberton DK, et al. Body size and allometric variation in facial shape in children. Am J Phys Anthropol. 2018;165(2):327-42. Epub 2017/11/27. doi: 10.1002/ajpa.23356. PubMed PMID: 29178597; PubMed Central PMCID: PMCPMC5777898.
65. Goios A, Pereira L, Bogue M, Macaulay V, Amorim A. mtDNA phylogeny and evolution of laboratory mouse strains. Genome Res. 2007;17(3):293-8. Epub 2007/02/06. doi: 10.1101/gr.5941007. PubMed PMID: 17284675; PubMed Central PMCID: PMCPMC1800920.
66. Logan RW, Robledo RF, Recla JM, Philip VM, Bubier JA, Jay JJ, et al. High-precision genetic mapping of behavioral traits in the diversity outbred mouse population. Genes Brain Behav. 2013;12(4):424-37. Epub 2013/03/20. doi: 10.1111/gbb.12029. PubMed PMID: 23433259; PubMed Central PMCID: PMCPMC3709837.
67. French JE, Gatti DM, Morgan DL, Kissling GE, Shockley KR, Knudsen GA, et al. Diversity Outbred Mice Identify Population-Based Exposure Thresholds and Genetic Factors that Influence Benzene-Induced Genotoxicity. Environ Health Perspect. 2015;123(3):237-45. Epub 2014/11/06. doi: 10.1289/ehp.1408202. PubMed PMID: 25376053; PubMed Central PMCID: PMCPMC4348743.
68. Smallwood TL, Gatti DM, Quizon P, Weinstock GM, Jung KC, Zhao L, et al. High-resolution genetic mapping in the diversity outbred mouse population identifies Apobec1 as a candidate gene for atherosclerosis. G3 (Bethesda). 2014;4(12):2353-63. Epub 2014/10/23. doi: 10.1534/g3.114.014704. PubMed PMID: 25344410; PubMed Central PMCID: PMCPMC4267931.
69. Shorter JR, Huang W, Beak JY, Hua K, Gatti DM, de Villena FP, et al. Quantitative trait mapping in Diversity Outbred mice identifies two genomic regions associated with heart size. Mamm Genome. 2018;29(1-2):80-9. Epub 2017/12/26. doi: 10.1007/s00335-017-9730-7. PubMed PMID: 29279960; PubMed Central PMCID: PMCPMC6340297.
70. Bressler J, Tsai TF, Wu MY, Tsai SF, Ramirez MA, Armstrong D, et al. The SNRPN promoter is not required for genomic imprinting of the Prader-Willi/Angelman domain in mice. Nat Genet. 2001;28(3):232-40. doi: 10.1038/90067. PubMed PMID: 11431693.
71. Albrecht U, Sutcliffe JS, Cattanach BM, Beechey CV, Armstrong D, Eichele G, et al. Imprinted expression of the murine Angelman syndrome gene, Ube3a, in hippocampal and Purkinje neurons. Nat Genet. 1997;17(1):75-8. doi: 10.1038/ng0997-75. PubMed PMID: 9288101.
72. Kobayashi S, Kohda T, Ichikawa H, Ogura A, Ohki M, Kaneko-Ishino T, et al. Paternal expression of a novel imprinted gene, Peg12/Frat3, in the mouse 7C region homologous to the Prader-Willi syndrome region. Biochem Biophys Res Commun. 2002;290(1):403-8. doi: 10.1006/bbrc.2001.6160. PubMed PMID: 11779183.
73. Morison IM, Ramsay JP, Spencer HG. A census of mammalian imprinting. Trends Genet. 2005;21(8):457-65. doi: 10.1016/j.tig.2005.06.008. PubMed PMID: 15990197.
74. Gray TA, Saitoh S, Nicholls RD. An imprinted, mammalian bicistronic transcript encodes two independent proteins. Proc Natl Acad Sci U S A. 1999;96(10):5616-21. doi: 10.1073/pnas.96.10.5616. PubMed PMID: 10318933; PubMed Central PMCID: PMCPMC21909.
75. Knoll JH, Nicholls RD, Magenis RE, Graham JM, Lalande M, Latt SA. Angelman and Prader-Willi syndromes share a common chromosome 15 deletion but differ in parental origin

773 of the deletion. Am J Med Genet. 1989;32(2):285-90. doi: 10.1002/ajmg.1320320235. PubMed
774 PMID: 2564739.
775 76. Mic FA, Molotkov A, Fan X, Cuenca AE, Duester G. RALDH3, a retinaldehyde
776 dehydrogenase that generates retinoic acid, is expressed in the ventral retina, otic vesicle and
777 olfactory pit during mouse development. Mech Dev. 2000;97(1-2):227-30. doi: 10.1016/s0925-
778 4773(00)00434-2. PubMed PMID: 11025231.
779 77. Visel A, Thaller C, Eichele G. GenePaint.org: an atlas of gene expression patterns in the
780 mouse embryo. Nucleic Acids Res. 2004;32(Database issue):D552-6. doi: 10.1093/nar/gkh029.
781 PubMed PMID: 14681479; PubMed Central PMCID: PMCPMC308763.
782 78. Martin KM, Metcalfe JC, Kemp PR. Expression of Klf9 and Klf13 in mouse development.
783 Mech Dev. 2001;103(1-2):149-51. doi: 10.1016/s0925-4773(01)00343-4. PubMed PMID:
784 11335124.
785 79. Yokoyama S, Ito Y, Ueno-Kudoh H, Shimizu H, Uchibe K, Albini S, et al. A systems
786 approach reveals that the myogenesis genome network is regulated by the transcriptional
787 repressor RP58. Dev Cell. 2009;17(6):836-48. doi: 10.1016/j.devcel.2009.10.011. PubMed PMID:
788 20059953; PubMed Central PMCID: PMCPMC3110151.
789 80. Unda FJ, Pérez-Nanclares G, Le Morvan V, Hernández C, Vilaxa A, De-la-Fuente M, et al.
790 Dynamic assembly of tight junction-associated proteins ZO-1, ZO-2, ZO-3 and occludin during
791 mouse tooth development. Histol Histopathol. 2003;18(1):27-38. doi: 10.14670/HH-18.27.
792 PubMed PMID: 12507281.
793 81. Yoshida T, Miyoshi J, Takai Y, Thesleff I. Cooperation of nectin-1 and nectin-3 is required
794 for normal ameloblast function and crown shape development in mouse teeth. Dev Dyn.
795 2010;239(10):2558-69. doi: 10.1002/dvdy.22395. PubMed PMID: 21038445.
796 82. de Koning DJ, Bovenhuis H, van Arendonk JA. On the detection of imprinted quantitative
797 trait loci in experimental crosses of outbred species. Genetics. 2002;161(2):931-8. PubMed
798 PMID: 12072486; PubMed Central PMCID: PMCPMC1462155.
799 83. Cheverud JM, Hager R, Roseman C, Fawcett G, Wang B, Wolf JB. Genomic imprinting
800 effects on adult body composition in mice. Proc Natl Acad Sci U S A. 2008;105(11):4253-8. Epub
801 2008/03/12. doi: 10.1073/pnas.0706562105. PubMed PMID: 18337500; PubMed Central
802 PMCID: PMCPMC2393747.
803 84. Leamy LJ, Klingenberg CP, Sherratt E, Wolf JB, Cheverud JM. A search for quantitative
804 trait loci exhibiting imprinting effects on mouse mandible size and shape. Heredity (Edinb).
805 2008;101(6):518-26. Epub 2008/08/06. doi: 10.1038/hdy.2008.79. PubMed PMID: 18685568.
806 85. Holm VA, Cassidy SB, Butler MG, Hanchett JM, Greenswag LR, Whitman BY, et al.
807 Prader-Willi syndrome: consensus diagnostic criteria. Pediatrics. 1993;91(2):398-402. PubMed
808 PMID: 8424017; PubMed Central PMCID: PMCPMC6714046.
809 86. Katz DC, Grote MN, Weaver TD. Changes in human skull morphology across the
810 agricultural transition are consistent with softer diets in preindustrial farming groups. Proc Natl
811 Acad Sci U S A. 2017;114(34):9050-5. Epub 2017/07/24. doi: 10.1073/pnas.1702586114.
812 PubMed PMID: 28739900; PubMed Central PMCID: PMCPMC5576786.
813 87. Liberzon A, Subramanian A, Pinchback R, Thorvaldsdóttir H, Tamayo P, Mesirov JP.
814 Molecular signatures database (MSigDB) 3.0. Bioinformatics. 2011;27(12):1739-40. Epub
815 2011/05/05. doi: 10.1093/bioinformatics/btr260. PubMed PMID: 21546393; PubMed Central
816 PMCID: PMCPMC3106198.

817 88. Le N, Nagarajan R, Wang JY, Svaren J, LaPash C, Araki T, et al. Nab proteins are essential
818 for peripheral nervous system myelination. Nat Neurosci. 2005;8(7):932-40. PubMed PMID:
819 16136673.
820 89. Shi C, Sakuma M, Mooroka T, Liscoe A, Gao H, Croce KJ, et al. Down-regulation of the
821 forkhead transcription factor Foxp1 is required for monocyte differentiation and macrophage
822 function. Blood. 2008;112(12):4699-711. Epub 2008/09/17. doi: 10.1182/blood-2008-01-
823 137018. PubMed PMID: 18799727; PubMed Central PMCID: PMCPMC2597137.
824 90. Zhao H, Zhou W, Yao Z, Wan Y, Cao J, Zhang L, et al. Foxp1/2/4 regulate endochondral
825 ossification as a suppresser complex. Dev Biol. 2015;398(2):242-54. Epub 2014/12/17. doi:
826 10.1016/j.ydbio.2014.12.007. PubMed PMID: 25527076; PubMed Central PMCID:
827 PMCPMC4342236.
828 91. Pacheco-Costa R, Kadakia JR, Atkinson EG, Wallace JM, Plotkin LI, Reginato RD.
829 Connexin37 deficiency alters organic bone matrix, cortical bone geometry, and increases
830 Wnt/β-catenin signaling. Bone. 2017;97:105-13. Epub 2017/01/16. doi:
831 10.1016/j.bone.2017.01.010. PubMed PMID: 28096061.
832 92. Wilson DG, Phamluong K, Lin WY, Barck K, Carano RA, Diehl L, et al. Chondroitin sulfate
833 synthase 1 (Chsy1) is required for bone development and digit patterning. Dev Biol.
834 2012;363(2):413-25. Epub 2012/01/17. doi: 10.1016/j.ydbio.2012.01.005. PubMed PMID:
835 22280990.
836 93. Xing WR, Goodluck H, Zeng C, Mohan S. Role and mechanism of action of leucine-rich
837 repeat kinase 1 in bone. Bone Res. 2017;5:17003. Epub 2017/03/14. doi:
838 10.1038/boneres.2017.3. PubMed PMID: 28326224; PubMed Central PMCID:
839 PMCPMC5348726.
840 94. Vecchione L, Byron C, Cooper GM, Barbano T, Hamrick MW, Sciote JJ, et al. Craniofacial
841 morphology in myostatin-deficient mice. J Dent Res. 2007;86(11):1068-72. doi:
842 10.1177/154405910708601109. PubMed PMID: 17959898.
843 95. Vecchione L, Miller J, Byron C, Cooper GM, Barbano T, Cray J, et al. Age-related changes
844 in craniofacial morphology in GDF-8 (myostatin)-deficient mice. Anat Rec (Hoboken).
845 2010;293(1):32-41. doi: 10.1002/ar.21024. PubMed PMID: 19899116; PubMed Central PMCID:
846 PMCPMC3113544.
847 96. Sahni M, Ambrosetti DC, Mansukhani A, Gertner R, Levy D, Basilico C. FGF signaling
848 inhibits chondrocyte proliferation and regulates bone development through the STAT-1
849 pathway. Genes & Development. 1999;13:1361-6.
850 97. Xiao L, Naganawa T, Obugunde E, Gronowicz G, Ornitz DM, Coffin JD, et al. Stat1
851 controls postnatal bone formation by regulating fibroblast growth factor signaling in
852 osteoblasts. J Biol Chem. 2004;279(26):27743-52. Epub 2004/04/08. doi:
853 10.1074/jbc.M314323200. PubMed PMID: 15073186.
854 98. Kim S, Koga T, Isobe M, Kern BE, Yokochi T, Chin YE, et al. Stat1 functions as a
855 cytoplasmic attenuator of Runx2 in the transcriptional program of osteoblast differentiation.
856 Genes Dev. 2003;17(16):1979-91. doi: 10.1101/gad.1119303. PubMed PMID: 12923053;
857 PubMed Central PMCID: PMCPMC196253.
858 99. Le Fevre AK, Taylor S, Malek NH, Horn D, Carr CW, Abdul-Rahman OA, et al. FOXP1
859 mutations cause intellectual disability and a recognizable phenotype. Am J Med Genet A.

860 2013;161A(12):3166-75. Epub 2013/09/24. doi: 10.1002/ajmg.a.36174. PubMed PMID:
861 24214399.
862 100. Tian J, Ling L, Shboul M, Lee H, O'Connor B, Merriman B, et al. Loss of CHSY1, a secreted
863 FRINGE enzyme, causes syndromic brachydactyly in humans via increased NOTCH signaling. Am
864 J Hum Genet. 2010;87(6):768-78. doi: 10.1016/j.ajhg.2010.11.005. PubMed PMID: 21129727;
865 PubMed Central PMCID: PMCPMC2997365.
866 101. Huh A, Horton MJ, Cuenco KT, Raoul G, Rowlerson AM, Ferri J, et al. Epigenetic influence
867 of KAT6B and HDAC4 in the development of skeletal malocclusion. Am J Orthod Dentofacial
868 Orthop. 2013;144(4):568-76. doi: 10.1016/j.ajodo.2013.06.016. PubMed PMID: 24075665;
869 PubMed Central PMCID: PMCPMC3849704.
870 102. Vimalraj S, Arumugam B, Miranda PJ, Selvamurugan N. Runx2: Structure, function, and
871 phosphorylation in osteoblast differentiation. Int J Biol Macromol. 2015;78:202-8. Epub
872 2015/04/13. doi: 10.1016/j.ijbiomac.2015.04.008. PubMed PMID: 25881954.
873 103. Clayton-Smith J, O'Sullivan J, Daly S, Bhaskar S, Day R, Anderson B, et al. Whole-exome-
874 sequencing identifies mutations in histone acetyltransferase gene KAT6B in individuals with the
875 Say-Barber-Biesecker variant of Ohdo syndrome. Am J Hum Genet. 2011;89(5):675-81. doi:
876 10.1016/j.ajhg.2011.10.008. PubMed PMID: 22077973; PubMed Central PMCID:
877 PMCPMC3213399.
878 104. Sena K, Morotome Y, Baba O, Terashima T, Takano Y, Ishikawa I. Gene expression of
879 growth differentiation factors in the developing periodontium of rat molars. J Dent Res.
880 2003;82(3):166-71. doi: 10.1177/154405910308200304. PubMed PMID: 12598543.
881 105. Nakashima M, Toyono T, Murakami T, Akamine A. Transforming growth factor-beta
882 superfamily members expressed in rat incisor pulp. Arch Oral Biol. 1998;43(9):745-51. doi:
883 10.1016/s0003-9969(98)00046-6. PubMed PMID: 9783830.
884 106. Cerny R, Cattell M, Sauka-Spengler T, Bronner-Fraser M, Yu F, Medeiros DM. Evidence
885 for the prepattern/cooption model of vertebrate jaw evolution. Proc Natl Acad Sci U S A.
886 2010;107(40):17262-7. Epub 2010/09/20. doi: 10.1073/pnas.1009304107. PubMed PMID:
887 20855630; PubMed Central PMCID: PMCPMC2951391.
888 107. So PL, Danielian PS. Cloning and expression analysis of a mouse gene related to
889 Drosophila odd-skipped. Mech Dev. 1999;84(1-2):157-60. PubMed PMID: 10473132.
890 108. Kawai S, Yamauchi M, Amano A. Zinc-finger transcription factor Odd-skipped related 1
891 regulates cranial bone formation. J Bone Miner Metab. 2018;36(6):640-7. Epub 2017/12/12.
892 doi: 10.1007/s00774-017-0885-9. PubMed PMID: 29234951.
893 109. Jeong J, Cesario J, Zhao Y, Burns L, Westphal H, Rubenstein JL. Cleft palate defect of
894 Dlx1/2-/- mutant mice is caused by lack of vertical outgrowth in the posterior palate. Dev Dyn.
895 2012;241(11):1757-69. Epub 2012/09/28. doi: 10.1002/dvdy.23867. PubMed PMID: 22972697;
896 PubMed Central PMCID: PMCPMC3988582.
897 110. Zelzer E, McLean W, Ng YS, Fukai N, Reginato AM, Lovejoy S, et al. Skeletal defects in
898 VEGF(120/120) mice reveal multiple roles for VEGF in skeletogenesis. Development.
899 2002;129(8):1893-904. PubMed PMID: 11934855.
900 111. R Development Core Team. R: A language and environment for statistical computing. R
901 Foundation for Statistical Computing, Vienna, Austria. URL http://www.R-project.org/2015.
902 112. Mitteroecker P, Gunz P. Advances in Geometric Morphometrics. Evolutionary Biology.
903 2009;36(2):235-47. doi: 10.1007/s11692-009-9055-x.

113. Schlager S. Morpho and Rvcg – Shape Analysis in R. In: Zheng G, Li S, Szekely G, editors. Statistical Shape and Deformation Analysis: Academic Press; 2017. p. 217-56.
114. Mardia KV, Bookstein FL, Moreton IJ. Statistical assessment of bilateral symmetry of shapes. Biometrika. 2000;87(2):285-300.
115. Klingenberg CP, Barluenga M, Meyer A. Shape analysis of symmetric structures: quantifying variation among individuals and asymmetry. Evolution. 2002;56(10):1909-20. PubMed PMID: 12449478.
116. Morgan AP, Fu CP, Kao CY, Welsh CE, Didion JP, Yadgary L, et al. The Mouse Universal Genotyping Array: From Substrains to Subspecies. G3 (Bethesda). 2015;6(2):263-79. Epub 2015/12/18. doi: 10.1534/g3.115.022087. PubMed PMID: 26684931; PubMed Central PMCID: PMCPMC4751547.
117. Didion JP, Morgan AP, Clayshulte AM, Mcmullan RC, Yadgary L, Petkov PM, et al. A multi-megabase copy number gain causes maternal transmission ratio distortion on mouse chromosome 2. PLoS Genet. 2015;11(2):e1004850. Epub 2015/02/13. doi: 10.1371/journal.pgen.1004850. PubMed PMID: 25679959; PubMed Central PMCID: PMCPMC4334553.
118. Cardon LR, Palmer LJ. Population stratification and spurious allelic association. Lancet. 2003;361(9357):598-604. doi: 10.1016/S0140-6736(03)12520-2. PubMed PMID: 12598158.
119. Broman KW, Gatti DM, Svenson KL, Sen Ś, Churchill GA. Cleaning Genotype Data from Diversity Outbred Mice. G3 (Bethesda). 2019;9(5):1571-9. Epub 2019/05/07. doi: 10.1534/g3.119.400165. PubMed PMID: 30877082; PubMed Central PMCID: PMCPMC6505173.
120. Sybert VP, McCauley E. Turner's syndrome. N Engl J Med. 2004;351(12):1227-38. doi: 10.1056/NEJMra030360. PubMed PMID: 15371580.
121. Hallgrimsson BA, J David, Katz DC, Bannister JJ, Riccardi SL, Mahasuwan N, McInnes BL, et al. Automated syndrome diagnosis by three-dimensional facial photogrammetric imaging. American Journal of Human Genetics. 2019, in review.
122. Krzanowski WJ. Principles of Multivariate Analysis: A User's Perspective. New York: Oxford University Press; 2005.
123. Churchill GA, Doerge RW. Empirical threshold values for quantitative trait mapping. Genetics. 1994;138(3):963-71. PubMed PMID: 7851788; PubMed Central PMCID: PMCPMC1206241.
124. Manichaikul A, Dupuis J, Sen S, Broman KW. Poor performance of bootstrap confidence intervals for the location of a quantitative trait locus. Genetics. 2006;174(1):481-9. Epub 2006/06/18. doi: 10.1534/genetics.106.061549. PubMed PMID: 16783000; PubMed Central PMCID: PMCPMC1569776.
125. Yalcin B, Flint J, Mott R. Using progenitor strain information to identify quantitative trait nucleotides in outbred mice. Genetics. 2005;171(2):673-81. Epub 2005/08/05. doi: 10.1534/genetics.104.028902. PubMed PMID: 16085706; PubMed Central PMCID: PMCPMC1456780.
126. Baud A, Hermsen R, Guryev V, Stridh P, Graham D, McBride MW, et al. Combined sequence-based and genetic mapping analysis of complex traits in outbred rats. Nat Genet. 2013;45(7):767-75. Epub 2013/05/26. doi: 10.1038/ng.2644. PubMed PMID: 23708188; PubMed Central PMCID: PMCPMC3821058.

127. Rhee SY, Wood V, Dolinski K, Draghici S. Use and misuse of the gene ontology annotations. Nat Rev Genet. 2008;9(7):509-15. Epub 2008/05/13. doi: 10.1038/nrg2363. PubMed PMID: 18475267.
128. Maglott D, Ostell J, Pruitt KD, Tatusova T. Entrez Gene: gene-centered information at NCBI. Nucleic Acids Res. 2011;39(Database issue):D52-7. Epub 2010/11/28. doi: 10.1093/nar/gkq1237. PubMed PMID: 21115458; PubMed Central PMCID: PMCPMC3013746.
129. Subramanian A, Tamayo P, Mootha VK, Mukherjee S, Ebert BL, Gillette MA, et al. Gene set enrichment analysis: a knowledge-based approach for interpreting genome-wide expression profiles. Proc Natl Acad Sci U S A. 2005;102(43):15545-50. Epub 2005/09/30. doi: 10.1073/pnas.0506580102. PubMed PMID: 16199517; PubMed Central PMCID: PMCPMC1239896.
130. Katz DC, Grote MN, Weaver TD. A mixed model for the relationship between climate and cranial form. American Journal of Physical Anthropology. 2016;160:593-603.
131. Mitteroecker P, Cheverud JM, Pavlicev M. Multivariate Analysis of Genotype-Phenotype Association. Genetics. 2016. doi: 10.1534/genetics.115.181339.
132. Nakagawa S, Schielzeth H. A general and simple method for obtaining R^2 from generalized linear mixed-effects models. Methods in Ecology and Evolution. 2013;4:133-42. doi: 10.1111/j.2041-210x.2012.00261.x.
133. Adler D, Murdoch D, others. rgl: 3D Visualization Using OpenGL. 0.95.1441 ed2016.
134. Rohlf FJ. Shape statistics: Procrustes superimpositions and tangent spaces. Journal of Classification. 1999;16(2):197-223.

Supporting Information

S1 Fig. Eigenvalue decay. Percentage of total variation explained for each shape principal component. We performed genome scans for all PCs explaining more than 1% of shape variation (red point identifies cutoff at PC 20) and subjected the first five PCs (green point identifies PC 5 floor) to in-depth analysis.

S2 Fig. Change in chromosome 2 WSB allele frequencies over generations. Sample-wide WSB allele frequency on chromosome 2 by DO generation. The high WSB allele frequency in earlier generations reflects meiotic drive for WSB at the *R2d2* locus. Declining frequencies in later generations reflect the systematic purge of WSB alleles from the DO population.

S1 Table. LOD peaks and support intervals for all QTL on PCs 1-20.

979 **S2 Table.** Full array of LOCO mean heritabilities over PCs 1-20.

980 **S1 File. Genes, PCs 1-5.** All named, protein-coding genes in the PC 1-5 QTL intervals.

981 **S2 File. Top GO annotations, PCs 1-5.** Top 100 FDR q-value GO terms for the PC 1-5 QTL interval

982 gene set (Molecular Signatures Database output file).

983 **S3 File. Top GO annotations, PC 1.** For the PC1 QTL interval gene set, GO terms with FDR q-

984 value < 0.05 (Molecular Signatures Database output file).

985